

RESEARCH ARTICLE

10.1002/2016JE005061

Key Points:

- A new model for canyon formation through waterfall retreat combines flood hydraulics and erosional mechanics
- The model is used as a paleohydraulic tool to estimate the discharge of megafloods on Earth and Mars
- Compared with previous estimates, predicted discharges are lower, durations higher, and water volumes are similar

Correspondence to:

M. G. A. Lapotre,
mlapotre@caltech.edu

Citation:

Lapotre, M. G. A., M. P. Lamb, and R. M. E. Williams (2016), Canyon formation constraints on the discharge of catastrophic outburst floods of Earth and Mars, *J. Geophys. Res. Planets*, 121, 1232–1263, doi:10.1002/2016JE005061.

Received 22 APR 2016

Accepted 10 JUN 2016

Accepted article online 13 JUN 2016

Published online 9 JUL 2016

Corrected 17 AUG 2016

This article was corrected on 17 AUG 2016. See the end of the full text for details.

Canyon formation constraints on the discharge of catastrophic outburst floods of Earth and Mars

Mathieu G. A. Lapotre¹, Michael P. Lamb¹, and Rebecca M. E. Williams²¹Division of Geological and Planetary Sciences, California Institute of Technology, Pasadena, California, USA, ²Planetary Science Institute, Tucson, Arizona, USA

Abstract Catastrophic outburst floods carved amphitheater-headed canyons on Earth and Mars, and the steep headwalls of these canyons suggest that some formed by upstream headwall propagation through waterfall erosion processes. Because topography evolves in concert with water flow during canyon erosion, we suggest that bedrock canyon morphology preserves hydraulic information about canyon-forming floods. In particular, we propose that for a canyon to form with a roughly uniform width by upstream headwall retreat, erosion must occur around the canyon head, but not along the sidewalls, such that canyon width is related to flood discharge. We develop a new theory for bedrock canyon formation by megafloods based on flow convergence of large outburst floods toward a horseshoe-shaped waterfall. The model is developed for waterfall erosion by rock toppling, a candidate erosion mechanism in well fractured rock, like columnar basalt. We apply the model to 14 terrestrial (Channeled Scablands, Washington; Snake River Plain, Idaho; and Ásbyrgi canyon, Iceland) and nine Martian (near Ares Vallis and Echus Chasma) bedrock canyons and show that predicted flood discharges are nearly 3 orders of magnitude less than previously estimated, and predicted flood durations are longer than previously estimated, from less than a day to a few months. Results also show a positive correlation between flood discharge per unit width and canyon width, which supports our hypothesis that canyon width is set in part by flood discharge. Despite lower discharges than previously estimated, the flood volumes remain large enough for individual outburst floods to have perturbed the global hydrology of Mars.

1. Introduction

The largest floods in the solar system are inferred to have occurred from the dramatic imprint they have left on the landscapes of Earth and Mars and in particular from the presence of large bedrock canyons on both planets. For example, on Earth, the Big Lost River and Bonneville floods carved canyons along the Pleistocene Snake River valley [Malde, 1960; Scott, 1982; O'Connor, 1993; Rathburn, 1993] (Figures 1a–1c), and the glacial outburst Missoula floods carved the Pleistocene Channeled Scablands of the northwestern United States [e.g., Bretz, 1969; Baker, 1973; O'Connor and Baker, 1992] (Figures 1e–1g). Some of the largest floods on Mars carved the outflow channels of the circum-Chryse region, for example, at Ares Vallis [Komatsu and Baker, 1997; Pacifici et al., 2009; Warner et al., 2010] (Figure 1i) and Kasei Valles [Robinson and Tanaka, 1990; Williams et al., 2000; Williams and Malin, 2004]. Two remaining outstanding unknowns are the water discharges associated with these floods and the duration of the flood events. A better quantitative understanding of these floods is critical because (1) they are unlike anything we observe today, (2) they were so large that they may have altered global hydrology and climate on both planets [e.g., Baker, 2002], and (3) they represent one of the best indicators of flowing water during the decline of surface hydrology on Mars [e.g., Carr and Head, 2010].

Paleohydrologists mostly use two methods to infer discharge from canyon observations: (1) they calculate the required flow depth to initiate motion of the observed sediment sizes through a Shields stress criterion [e.g., O'Connor, 1993; Lamb et al., 2008, 2014] or (2) they assume that observed channels or canyons were filled to the brim (brimful assumption) [e.g., Baker and Milton, 1974; Carr, 1979; Robinson and Tanaka, 1990; Komatsu and Baker, 1997; McIntyre et al., 2012]. Initial motion and brimful assumptions provide conservative lower and upper bounds on flow discharge, respectively, constraining its value with an uncertainty of many orders of magnitude.

Flow durations have been previously estimated from either (1) water discharge and eroded rock volume (assuming a water-to-rock ratio for erosion) [e.g., Komar, 1980; Carr, 1986; Leask et al., 2007] or (2) sediment

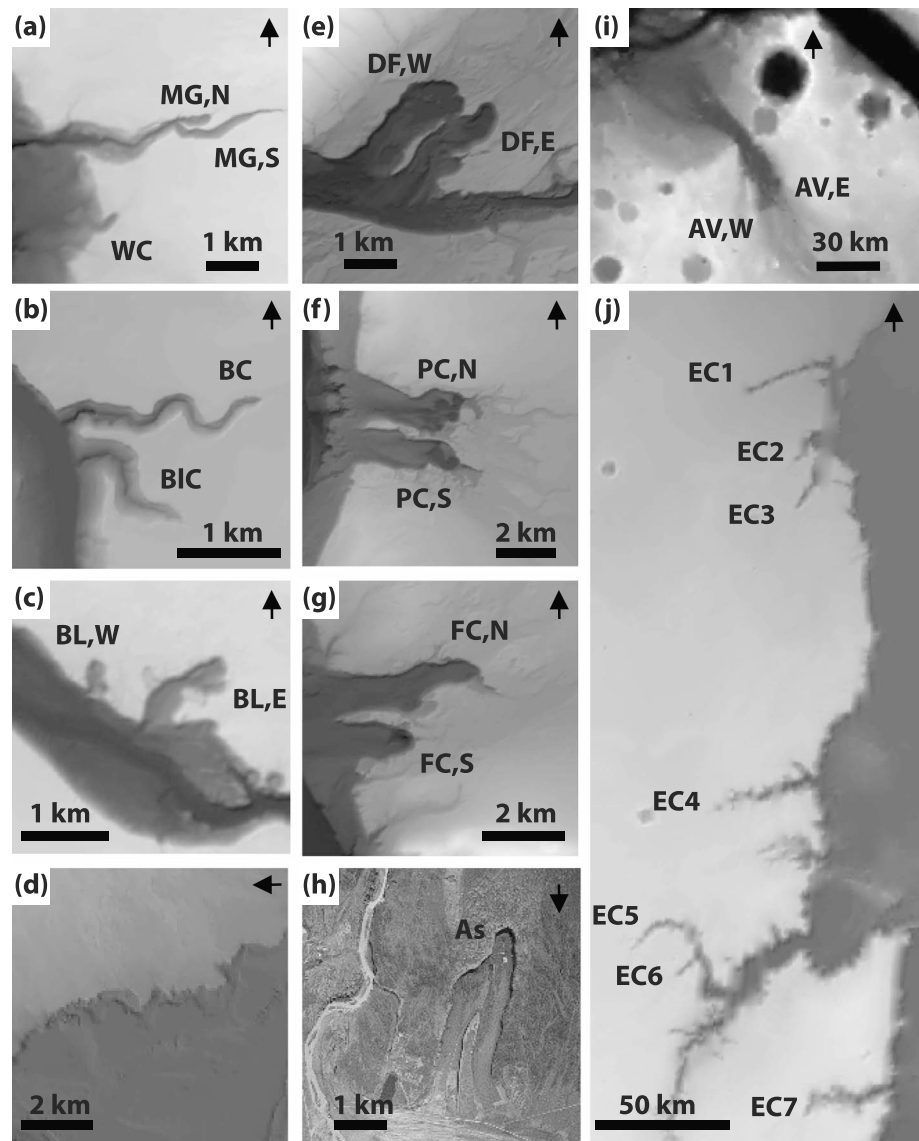


Figure 1. (a) Malad Gorge (MG,N and MG,S) and Woody’s Cove (WC), Idaho (ASTER); (b) Box Canyon (BC) and Blind Canyon (BIC), Idaho (ASTER); (c) Blue Lakes (BL,W and BL,E), Idaho (ASTER); (d) escarpment downstream of Malad Gorge, Idaho (SRTM); (e) Dry Falls (DF,W and DF,E), Washington (ASTER); (f) Pothole Coulee (PC,N and PC,S), Washington (ASTER); (g) Frenchman Coulee (FC,N and FC,S), Washington (ASTER); (h) Ásbyrgi canyon (As), Iceland (Aerial photograph source: Landmælingar Íslands); (i) canyons near Echus Chasma (EC1–EC7), Mars (MOLA); and (j) dry cataract near Ares Vallis (AV,E and AV,W), Mars (MOLA). Arrows indicate the north direction.

transport capacity and the volume of eroded rock assuming transport-limited conditions [e.g., *Lamb et al., 2008; Lamb and Fonstad, 2010*]. Both methods require a priori knowledge of flow depth. In the absence of better estimates, flow depth has generally been assumed to be brimful, which leads to flood durations that are likely largely underestimated and thus provide lower bounds.

While estimates of flood discharges and durations have been made from assumptions about flood hydraulics, we herein propose that tighter constraints can come specifically from coupling hydraulics to erosion mechanics. An important, but largely unutilized characteristic of flood-carved canyons in basalt is that they often have steep amphitheater-shaped headwalls [e.g., *Lamb et al., 2006*]. In particular, amphitheater-headed canyons that have roughly uniform widths are thought to form by upstream propagation of the headwall [*Lamb and Dietrich, 2009; Petroff et al., 2011*]. In the absence of quantitative mechanistic models for headwall

retreat, radically different flow configurations have been proposed to explain the formation of various amphitheater-headed canyons on Earth and Mars, such as both long-lived [Harrison and Grimm, 2005; Pelletier and Baker, 2011; Petroff et al., 2011] and catastrophic [Amidon and Clark, 2014] groundwater seepage erosion, as well as catastrophic overland flow and waterfall erosion [Baker and Milton, 1974; Carr, 1979; Komatsu and Baker, 1997; Lamb et al., 2006; Warner et al., 2010].

Canyons carved from groundwater seepage exist in cohesionless sediments on Earth [e.g., Pillans, 1985; Schumm et al., 1995; Luo et al., 1997], are debated in sedimentary rocks [Laity and Malin, 1985; Howard et al., 1987; Lamb et al., 2006], and are not observed in more crystalline lithologies [Lamb et al., 2006, 2007, 2008]. While mechanistic models combining both fluvial and mass wasting processes have been formulated for groundwater sapping in loose sediments [e.g., Howard and McLane, 1988], there is currently no tested theory for the mechanics of erosion by seepage in strong rocks. In contrast, canyons carved into crystalline bedrock likely form from waterfall erosion, either through undercutting in the plunge pool or through rock toppling at the waterfall brink [e.g., Gilbert, 1907; Haviv et al., 2006; Lamb et al., 2007; Lamb and Dietrich, 2009; Lamb et al., 2014].

Undercutting occurs as a result of scouring of rocks where the water jet impinges the plunge pool, by the combined mechanical action of water and transported sediments [Mason and Arumugam, 1985; Stein et al., 1993; Bollaert, 2004; Flores-Cervantes et al., 2006; Pagliara et al., 2006], while plucking and toppling occur through the action of bed shear stress applied by water flow upstream of the waterfall brink [e.g., Coleman et al., 2003; Chatanantavet and Parker, 2009; Lamb and Dietrich, 2009; Lamb et al., 2015]. In the case of vertically fractured lithologies, Lamb and Dietrich [2009] proposed that toppling of rock columns by overland flow could explain the morphology of amphitheater-headed canyons. Lamb et al. [2015] showed that toppling is the dominant erosion mechanism in fractured bedrock as long as block height is at least half of block width, which is typical of canyons carved in basalt with subvertical cooling joints, a common lithology in megaflood terrain on Earth and Mars. For example, toppling during large-scale floods is thought to have been the main mechanism for erosion at Box Canyon and Malad Gorge, Idaho [Lamb et al., 2008, 2014], and at Ásbyrgi in Iceland [Baynes et al., 2015a, 2015b]. On Mars, lava flows are ubiquitous [e.g., Christensen et al., 2000; Ruff and Christensen, 2002; Bibring et al., 2005; Ehlmann and Edwards, 2014], and basaltic columns were observed from orbit [Milazzo et al., 2009]. The ubiquity of fractured lithologies where bedrock canyons are found on Earth and Mars makes rock toppling a good candidate mechanism for the formation of canyons with amphitheater heads during large floods [e.g., Warner et al., 2010].

While mechanistic models for erosion are needed for both the groundwater and overland flood scenarios, we focus in this paper on toppling erosion because many canyons in fractured rock show evidence for this mechanism. Our intention is not to assert that all amphitheater canyons were formed by flood-driven block toppling but rather to demonstrate how canyons carved by this mechanism can be used as paleohydraulic indicators of past floods. We investigate the hypothesis that the width of amphitheater-headed (i.e., horseshoe-shaped) canyons carved by overland flow can be used as a proxy for water discharge of canyon-forming floods. We first build on a previous study of hydraulics upstream of horseshoe canyons and waterfalls [Lapotre and Lamb, 2015] and extend this work for bedrock canyon formation and dynamics. We then show how this model can be used as a paleohydraulic tool to predict the discharge of a canyon-carving flood. Finally, we apply the model to 23 terrestrial and Martian bedrock canyons and invert for discharge, Shields stress within the canyon, flood duration, and flood water volume.

2. Model for the Stability of Canyons and Escarpments

In order to form a canyon by upstream canyon-head retreat while maintaining a uniform width, geometry requires that erosion must occur at the upstream end of the canyon head, but not along the canyon sidewalls. Figure 2 illustrates our hypothesized formation mechanism. As a sheet flood of steady discharge flows over a planar landscape and approaches an escarpment, loss of hydrostatic pressure at the escarpment draws the water surface down toward embayments in the escarpment (Figure 2a). Due to flow focusing and enhanced shear stresses around their rim, embayments grow into canyons via block toppling and capture water away from neighboring canyons. The wining protocanyons both widen and lengthen (Figure 2b). This general competition mechanism is analogous to those proposed by Howard [1994] and Izumi and Parker [1995, 2000] for fluvially eroded escarpments and by Dunne [1990] for groundwater-dominated escarpment retreat. When the canyons are large enough to focus sufficient water into their heads, shear stresses along the sidewalls can drop below the threshold for erosion so that canyon widening stops, and the headwall retreats upstream

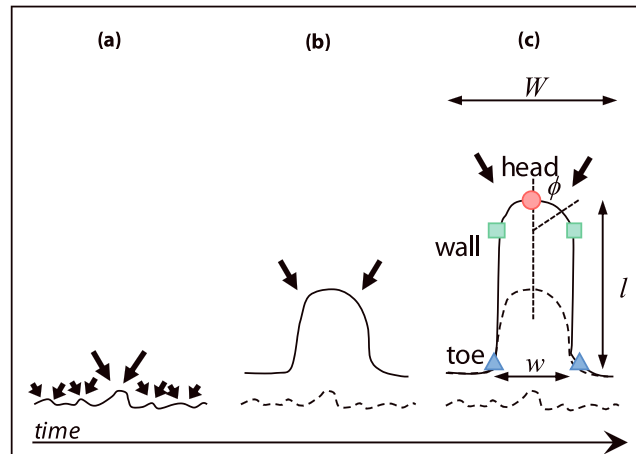


Figure 2. Hypothesis for the formation of bedrock canyons by knickpoint retreat. The sketches are in map view, with water flowing from top to bottom. Sinuous lines represent the geometry of the waterfall rim, and arrows indicate flow focusing into horseshoe-shaped embayments or canyon heads along the rim. (a) Water focuses toward horseshoe-shaped embayments along an otherwise linear escarpment. These embayments compete for water, until (b) one of them focuses enough water such that it captures most of the flow. The winning embayment is a protocanyon that both widens and lengthens, until (c) the canyon head focuses enough water for shear stresses along the sidewalls to drop below a critical value for erosion to occur. Past that stage, the canyon lengthens (increased l) through upstream retreat of the headwall, maintaining a roughly uniform width, w . The red circle indicates the location of the head, the green squares are at the location of the wall, and the blue triangles are at the location of the toe. The azimuth angle, ϕ , is defined as the angle between the canyon centerline and a line joining the center of the semi-circular head and a point along the rim of the headwall.

maintaining a roughly uniform width (Figure 2c). In this scenario, it is the distribution of bed shear stresses exerted by water along the waterfall rim that dictates the canyon width. Because bed shear stresses are set by the pattern of flow focusing around the canyon head, which itself is tied to the flood discharge [Lapotre and Lamb, 2015], we hypothesize that the width of the canyon head ultimately relates to flood discharge. More specifically, we hypothesize that, all else equal, larger floods produce wider canyons by this mechanism.

We focus on canyons formed by floods through upstream retreat of a headwall, where headwall erosion can be represented by a threshold erosion process, such as block toppling. Throughout our analysis we assume that the canyon topography evolves slowly relative to temporal changes in flow hydraulics so that the temporal acceleration terms in the equations of motion can be neglected during active canyon incision. This assumption is analogous to the quasi-steady assumption in fluvial morphodynamics and has been argued to hold when the volume of eroded or transported sediment is

small compared to the volume of water and hence that the sediment concentration is relatively dilute [de Vries, 1965]. In our analysis below we find that reconstructed sediment concentrations from megaflood-carved canyons are indeed small, ranging from 8×10^{-5} to 1×10^{-2} , which is in support of the quasi-steady assumption, but is also tied to our assumption that sediment is evacuated from canyons by fluvial transport. Canyons carved by concentrated debris flows or by a bore at the front of a flood wave may violate the quasi-steady assumption, for example, but most of the canyons of interest here show evidence of dilute fluvial transport such as imbricated boulders, boulder bars, streamlined islands, and terraces [e.g., Baker, 1973; Lamb et al., 2008; Warner et al., 2009; Baynes et al., 2015a]. Note that the quasi-steady assumption does not necessarily imply that the floods themselves were steady flows, only that the temporal acceleration terms can be neglected in the momentum budget. Following our conceptual model (Figure 2), we envision that non-steady behavior can emerge due to temporal changes in input flood discharge or through the evolution of canyon geometry during canyon formation. For example, an input flood discharge that decreases in time might result in a narrowing zone over which canyon headwall erosion occurs and hence a canyon with a systematic upstream decrease in width. In contrast, canyons that have relatively uniform widths are inferred to have formed under relatively steady flows.

In the rest of this section we develop theory to relate the discharge of a sheet flood to the shear stresses it imposes around the headwall of an amphitheater-headed canyon based on the steady-state hydraulic simulations of 2-D flow focusing from Lapotre and Lamb [2015]. We then use this theory in section 3 to relate the pattern of shear stresses around a canyon head to canyon formation by block toppling.

2.1. Discharge

Horseshoe-shaped waterfalls and canyons modify flow patterns upstream of the brink by accelerating water from steady, uniform flow conditions (e.g., where flow depth equals the normal flow depth, h_n) toward the

waterfall. For a steady flood over a planar, tilted plateau, this spatial acceleration leads to the formation of so-called drawdown profiles over a typical length scale of h_n/S , where S is the topographic gradient in the main flow direction [Bresse, 1866]. Downslope (i.e., in the direction of the topographic gradient) drawdown profiles develop for Froude subcritical floods only, while cross-slope (i.e., in the direction perpendicular to the topographic gradient) drawdown profiles develop for both subcritical and supercritical floods [Lapotre and Lamb, 2015]. Because of the development of these drawdown profiles, water is focused into the heads of canyons, and the total discharge within the head may be greater than the discharge integrated over an equivalent width far upstream of the waterfall where the flow is steady and uniform. From mass conservation, the discharge into a horseshoe-shaped canyon head is given by

$$Q_{h,2D} \equiv \frac{w}{2} \int_{\phi=-\pi/2}^{\pi/2} U_{0,2D}(\phi) h_{0,2D}(\phi) d\phi, \quad (1)$$

where w is the canyon width, ϕ is the azimuth angle with respect to the canyon centerline (Figure 2), $U_{0,2D}$ is the flow velocity component perpendicular to the rim of the horseshoe waterfall, and $h_{0,2D}$ is the flow depth at the rim.

The degree to which $Q_{h,2D}$ differs from the equivalent dimensional upstream discharge was addressed by Lapotre and Lamb [2015] and parametrized into a nondimensional canyon-head discharge for steady nonuniform flow, Q^* , such that

$$Q_{h,2D} = Q^* w q_n, \quad (2)$$

where q_n is the upstream discharge per unit width. The latter can be related to the upstream bed shear stress through conservation of mass and momentum. From conservation of mass for 1-D flow far upstream of the waterfall,

$$q_n = U_n h_n, \quad (3)$$

where the upstream normal flow velocity, U_n , is given by Manning's equation

$$U_n = \frac{h_n^{2/3} S^{1/2}}{n} \quad (4)$$

in which n is Manning's n . Combining equations (3) and (4) and conservation of momentum for steady and uniform flow,

$$\tau_n = \rho g h_n S, \quad (5)$$

where g is the acceleration of gravity, yields

$$q_n = \frac{1}{n S^{7/6}} \left(\frac{\tau_n}{\rho g} \right)^{5/3}. \quad (6)$$

Combining equations (2) and (6) yields a relation between the discharge into the canyon head and the upstream bed shear stress,

$$Q_{h,2D} = \frac{Q^* w}{n S^{7/6}} \left(\frac{\tau_n}{\rho g} \right)^{5/3}. \quad (7)$$

The normalized cumulative discharge to the canyon head, Q^* , is a dimensionless measure of how much the dimensional discharge into a horseshoe canyon head, $Q_{h,2D}$, is enhanced by flow focusing compared with the upstream normal flow discharge and depends on four dimensionless parameters, namely, the upstream Froude number, Fr_n , the canyon-width to flood-width ratio, $w^* = \frac{W}{W}$, where W is the flood width, the flood-width limitation factor, $W^* = \frac{(W-w)S}{2h_n}$, and the downslope backwater parameter, $l^* = \frac{lS}{h_n}$, where l is the canyon length (Figure 2) [Lapotre and Lamb, 2015].

Semiempirical relations, summarized in Appendix A, were determined by Lapotre and Lamb [2015] from simulations of steady, nonuniform sheet floods upstream of horseshoe waterfalls using ANUGA, a finite-volume modeling suite that solves the 2-D time-dependent depth-averaged shallow water equations [Roberts et al., 2009]. The key results are that floods with lower upstream Froude numbers, Fr_n , experience more convergence toward the rim of the waterfall. Escarpment length and width also affect the hydraulics upstream of the brink, for example, through the interaction of drawdown profiles and the edges of the flood.

In particular, when $W^* < 1$, lateral drawdown profiles do not reach a uniform flow depth near the edges of the flood, and flow acceleration is reduced in the direction perpendicular to the wall. Also, longer canyons loose more water over their sidewalls and have relatively less water at their toe (Figure 2).

According to our hypothesis, in order to form a canyon through canyon-head retreat while maintaining a roughly uniform width, the upstream discharge must be such that the shear stresses along the sidewalls are below the critical value for erosion, while the shear stress at the canyon head is above the critical value. In the following sections, we show how normal bed shear stress, τ_n , can be related to shear stress along the canyon rim.

2.1.1. Shear Stresses Along the Canyon Rim

Bed shear stress at the rim of a horseshoe waterfall, $\tau_{0,2D}$, can be written as

$$\tau_{0,2D} = \rho C_{f0,2D} U_{0,2D}^2, \quad (8a)$$

where ρ is the density of water and $C_{f0,2D} = \frac{n^2 g}{h_{0,2D}^{1/3}}$ is the friction coefficient at the canyon rim [e.g., *Stein and Julien*, 1993]. Flow velocity at the rim, $U_{0,2D}$, can be written in terms of the upstream normal flow velocity, U_n , such that equation (8a) becomes

$$\tau_{0,2D} = \rho C_{f0,2D} (\alpha_{2D} U_n)^2, \quad (8b)$$

in which $\alpha_{2D} \equiv \frac{U_{0,2D}}{U_n}$ is defined as the acceleration factor at the rim of a horseshoe waterfall [*Lapotre and Lamb*, 2015]. The acceleration factor at the rim of a horseshoe waterfall, α_{2D} , takes into account both lateral flow focusing and drawdown of the water surface in response to the loss of hydrostatic pressure at the waterfall. It can also be defined as

$$\alpha_{2D} \equiv \alpha^* \alpha_{1D}, \quad (9)$$

where $\alpha^* = \frac{\alpha_{2D}}{\alpha_{1D}}$ is the acceleration factor ratio defined in the work of *Lapotre and Lamb* [2015] that accounts for lateral flow focusing, and $\alpha_{1D} = \frac{U_{0,1D}}{U_n} = \frac{h_n}{h_{0,1D}}$, which accounts for drawdown in 1-D along the centerline, in which $U_{0,1D}$ and $h_{0,1D}$ are the flow velocity and depth at the brink of a linear escarpment, respectively. The 1-D acceleration factor, α_{1D} , is a function of the upstream Froude number only, with $\alpha_{1D} = \frac{1.4}{Fr_n^{3/2}}$ when $Fr_n \leq 1$ and $\alpha_{1D} = \frac{0.4 + Fr_n^2}{Fr_n^2}$ when $Fr_n > 1$ [*Rouse*, 1936; *Delleur et al.*, 1956; *Hager*, 1983]. The acceleration factor ratio, α^* , is a measure of the enhancement or decrease in flow acceleration at the brink of a horseshoe waterfall compared with that at a 1-D escarpment: for a linear escarpment, $\alpha^* = 1$, so that $\alpha_{2D} = \alpha_{1D}$, while at the center of a canyon head, $\alpha^* \geq 1$. *Lapotre and Lamb* [2015] evaluated α^* at three different locations around the rim of semicircular-headed canyons (Figure 2)—the head (upstream end of the canyon head, α_h^*), the wall (junction between the horseshoe head and the straight sidewall, α_w^*), and the toe (downstream end of the canyon sidewall, α_t^*). Analogous to the semiempirical relationships derived for Q^* , *Lapotre and Lamb* [2015] developed semiempirical relationships to predict the acceleration factor ratio, α^* . The semiempirical relationships for α^* were also derived using the same numerical simulations and are summarized in Appendix A.

Equations (8b) and (9) yield the shear stress along the canyon rim. We wish to relate these shear stress values to water discharge to use for paleohydraulic reconstruction. To do this, we combine equations (8b), (9), and Manning's equation (equation (4)) to express the bed shear stress at the rim of a horseshoe waterfall as

$$\tau_{0,2D} = \alpha_{1D}^{7/3} A^* \tau_n, \quad (10a)$$

in which A^* is defined here as the shear stress enhancement factor that is given by

$$A^* \equiv \frac{\tau_{0,2D}}{\alpha_{1D}^{7/3} \tau_n} = \alpha^{*2} \left(\frac{h_n}{\alpha_{1D} h_{0,2D}} \right)^{1/3}. \quad (10b)$$

The shear stress enhancement factor is the ratio of the shear stress at the rim of horseshoe waterfall, which takes into account both lateral flow focusing and drawdown of the water surface, relative to the shear stress at the rim of a linear escarpment. A^* is expected to vary around the canyon rim.

Equations (10a) and (10b) show that the upstream bed shear stress, τ_n , can be related to α_{1D} (which is a function of Fr_n), A^* and the bed shear stress at the canyon rim, $\tau_{0,2D}$, (which is unknown). The next steps are thus to determine A^* , which can be constrained from the flood simulations of *Lapotre and Lamb* [2015], and $\tau_{0,2D}$, which comes from canyon erosion mechanics (section 3).

2.1.2. Shear Stress Enhancement Factor

The shear stress enhancement factor, A^* , given by equation (10b), is a function of the acceleration factor ratio, α^* , which was determined by *Lapotre and Lamb* [2015], but also varies with the ratio of the flow depths at the canyon rim and upstream, which are unknown, but can be extracted from the simulations of *Lapotre and Lamb* [2015]. In these simulations, sheet floods were modeled over a tilted plateau and flow toward a waterfall with a semicircular head and a constant width. The domain geometry was analogous to that described in Figure 2c. At steady state, the flow velocity, $U_{0,2D}$, and depth, $h_{0,2D}$, were measured along the rim of a horseshoe waterfall as upstream Froude number (Fr_n), canyon-width to flood-width ratio (w^*), flood-width limitation factor (W^*), and downslope backwater parameter (I^*) were varied. We used these flow velocities and depths to calculate shear stress enhancement ratios at the canyon head (A_h^*) in the downslope direction, head-to-wall junction (A_w^*) in the cross-slope direction, and toe (A_t^*) in the downslope direction as a function of Fr_n , w^* , W^* , and I^* . We derive semiempirical relationships for the shear stress enhancement factor as a function of these parameters from 110 numerical simulations with different flood and canyon geometries following the technique described in *Lapotre and Lamb* [2015]. These relationships are summarized in Appendix B. Overall, the dependency of A^* on the aforementioned parameters is very similar to that of the acceleration factor ratios squared, described in *Lapotre and Lamb* [2015], due to the fact that $A^* \propto \alpha^{*2}$ (equation (10b)). We find that the effect of the additional depth factor makes A^* deviate from α^{*2} by up to 65% where flow thins significantly, for example, at the toe of the canyon, and should thus not be neglected.

2.1.3. Total Discharge Into the Canyon Head

The total discharge into the canyon head, $Q_{h,2D}$, that is required to generate a certain bed shear stress at the canyon rim, $\tau_{0,2D}$, finally can be estimated by combining equations (7) and (10a) and (10b) as

$$Q_{h,2D} = \frac{Q^* w}{n S^{7/6}} \left(\frac{\tau_{0,2D}}{\rho g \alpha_{1D}^{7/3} A^*} \right)^{5/3}. \quad (11)$$

All parameters in equation (11) can be estimated or calculated, except that of the shear stress value at the canyon rim during canyon formation, $\tau_{0,2D}$, which must come from erosion mechanics, and is discussed in section 3.

2.2. Total Flood Duration and Water Volume

Because we are interested in large catastrophic floods that rapidly erode large rock volumes, it is plausible that erosion of the headwall is limited by the rate at which flow within the canyon head can carry the eroded sediment out of the canyon [e.g., *Lamb and Fonstad*, 2010; *Lamb et al.*, 2014; *Lapotre and Lamb*, 2015]. If the flow cannot carry the eroded sediment away from the canyon head, talus will accumulate and buttress the headwall against further retreat [*Lamb et al.*, 2006]. We thus approximate the total cumulative duration of canyon-carving floods, T_f , by dividing the volume of eroded rock by the volumetric sediment flux from flow within the canyon, Q_{sc} [e.g., *Lamb and Fonstad*, 2010; *Lamb et al.*, 2015]. In addition to the transport-limitation assumption, we assume that the porosity of rock is zero and that flow width within the canyon is equal to the full canyon width. Under these assumptions, the total duration of canyon-carving floods is approximated by

$$T_f \approx \frac{IA_c}{Q_{sc}}, \quad (12)$$

in which $A_c = \gamma H_c w$ is the canyon cross-sectional area with γ being a shape factor varying between 0 and 1. Many canyons carved in basalt on Earth have rectangular cross sections [e.g., *Lamb et al.*, 2006], i.e., $\gamma = 1$. Martian canyons are thought to have formed billions of years ago [e.g., *Warner et al.*, 2010], and their geometries may have been significantly modified by subsequent mass wasting or periglacial processes making the original cross section difficult to constrain [e.g., *Head et al.*, 2006]. We thus assume a rectangular geometry. Equation (12) shows that a minimum estimate of total flood duration can be calculated from canyon length (l) and cliff height (H_c), which can both be measured, and sediment capacity per unit width ($q_{sc} = Q_{sc}/w$), which can be estimated from sediment transport theory. In the case of canyons formed by multiple floods, equation (12) represents the summed duration of all flood events that contributed to canyon formation.

Many empirical relationships exist to predict sediment capacity of bedload. In the following, we use that of *Fernandez Luque and Van Beek* [1976], i.e.,

$$q_{sc} = 5.7(Rgd^3)^{1/2}(\tau_* - \tau_{*c})^{3/2}, \quad (13)$$

where $R = \frac{(\rho_r - \rho)}{\rho}$, d is the grain diameter, and τ_* and τ_{*c} are the Shields and critical Shields stresses, respectively. The Shields stress [*Shields*, 1936] is the ratio of driving to resisting stresses acting on an eroded block, and we estimate it under the assumption of normal flow conditions (i.e., steady and uniform flow) within the canyon through

$$\tau_* = \frac{h_{nb}S_b}{Rd}, \quad (14)$$

where h_{nb} and S_b are the normal flow depth and bed slope in the canyon, respectively. The critical Shields stress, τ_{*c} , is a function of particle Reynolds number and reaches a value of ~ 0.045 for larger grains of interest here [e.g., *Miller et al.*, 1977; *Yalin and Karahan*, 1979].

We need to estimate flow depth within the canyon in order to calculate Shields stress downstream of the waterfall. Assuming again that flow is steady and uniform within the canyon, flow depth [e.g., *Chow*, 1959] is given by

$$h_{nb} = \left(\frac{nQ_{h,2D}}{wS_b^{1/2}} \right)^{3/5}, \quad (15)$$

where $Q_{h,2D}$ comes from equation (11). Our minimum bound on total flood duration thus can be calculated by combining equations (12)–(15) as

$$T_{f,\min} = \frac{IH_c}{5.7(Rgd^3)^{1/2} \left[\frac{S_b^{7/10}}{Rd} \left(\frac{nQ_{h,2D}}{w} \right)^{3/5} - 0.045 \right]^{3/2}}. \quad (16)$$

Finally, total water volume to the canyon head during canyon formation, V_{2D} , is obtained by multiplying the total discharge to the canyon head (equation (11)) by the total duration of canyon-carving floods (equation (16)), i.e.,

$$V_{2D} = Q_{h,2D}T_{f,\min}. \quad (17)$$

2.3. Comparison to Other Paleohydraulic Indicators

It is of interest to compare the results of our paleohydraulic method to more commonly used techniques. A lower bound on discharge per unit width in the canyon can be estimated by setting the Shields stress to its critical value for initiation of motion of the observed grain sizes on the bed. Consequently, the normal flow depth required to initiate sediment transport, h_i , can be estimated by setting $\tau_* = \tau_{*c}$ in equation (14), i.e., $h_i = (\tau_{*c}RD)/S_b$. Further, substituting for flow depth into equations (3) and (4) yields the corresponding normal discharge at incipient motion

$$Q_i = \frac{h_i^{5/3}S_b^{1/2}}{n}w. \quad (18)$$

Conversely, an upper bound on flow discharge may be estimated from the assumption that canyons were filled in to the brim. We define brimful flow depth, h_{bf} , as the thalweg depth, which is equal to H_c regardless of channel cross-sectional geometry. Corresponding discharges, Q_{bf} , can be calculated using equation (4) as

$$Q_{bf} = \frac{H_c^{5/3}S_b^{1/2}}{n}w. \quad (19)$$

It is not immediately clear how to calculate the duration of canyon incision under the brimful hypothesis because the hypothesis seems to require the existence of a canyon prior to the flood, or for the flood discharge to increase during progressive canyon incision, to maintain a brimful state. Nonetheless, total flood duration under the brimful hypothesis has been estimated previously by assuming transport-limited and brimful conditions ($h_{nb} = H_c$ in equation (14)) or by assuming a volumetric water-to-rock ratio, δ , and dividing

the estimated volume of water, $\delta l w H_c$, by the brimful water discharge, Q_{bf} (equation (19)) [e.g., Baker, 1973; Carr, 1996]. The water-to-rock ratio method was originally developed for hyperconcentrated flows (i.e., more than 40% sediment by weight or $\delta \geq 4.6$), which are relatively common in arid environments on Earth, and was argued to be relevant for Martian floods [Komar, 1980; Carr, 1996; Leask et al., 2007]. Corresponding water volumes are estimated by multiplying water discharge by total flood duration.

3. Erosion Constraints on Stable Width Canyons

In this section, we show how the discharge of canyon-carving floods, given by equation (11), can be constrained from what we know about flow focusing, the distribution of bed shear stresses, and rock toppling. In order to do so, we consider two different paleohydraulic constraints on flood discharge. The 2-D minimum-discharge model takes into account the effect of flow focusing and assumes that for erosion to occur, the critical shear stress for rock toppling, τ_c , must at least be attained where shear stress is the greatest, i.e., at the canyon head. Thus, $\tau_h = \tau_c$, in which τ_h is the value of $\tau_{0,2D}$ at the canyon head. The 2-D minimum-discharge model is similar to what was used by Lamb et al. [2014] and Baynes et al. [2015b], but they did not include 2-D flow focusing and instead assumed hydraulics for a 1-D escarpment. The 2-D maximum-discharge model assumes that the shear stress either at the wall, τ_w , or at the toe, τ_t , is at the threshold for toppling. In other words, $\max(\tau_w, \tau_t) = \tau_c$, where τ_w and τ_t are the values of $\tau_{0,2D}$ at the wall and toe, respectively. Otherwise, if $\tau_w > \tau_c$, the canyon would widen, or if $\tau_t > \tau_c$, both the canyon head and toe would erode, such that a preexisting canyon might not lengthen in time depending on the relative erosion rates at the head and toe. We thus expect the maximum-discharge model to be a better estimate of formative discharge in that it takes into account canyon formation considerations. The 2-D maximum model applies only to canyons that formed by upstream headwall retreat via block toppling while maintaining a roughly uniform width.

In order to apply the threshold models described above, we need to calculate $\tau_{0,2D}$ at the canyon head, wall, and toe. Rearranging equation (10b) and substituting for the shear stress enhancement factor at the canyon head, wall, and toe, respectively, we find

$$\tau_h = \alpha_{1D}^{7/3} A_h^* \tau_n, \quad (20a)$$

$$\tau_w = \alpha_{1D}^{7/3} A_w^* \tau_n, \quad (20b)$$

$$\tau_t = \alpha_{1D}^{7/3} A_t^* \tau_n, \quad (20c)$$

where the shear stress enhancement factors can be calculated from the relationships in Appendix B. Equations (20a)–(20c) are sole consequences of flow hydraulics as described in Lapotre and Lamb [2015] and do not assume any erosional mechanism. Erosional mechanics are incorporated into the model by setting the shear stress at the canyon head, wall, or toe equal to the critical shear stress for erosion, so that equations (20a)–(20c) becomes

$$\text{Minimum-discharge model: } \frac{\tau_n}{\tau_c} = \frac{1}{\alpha_{1D}^{7/3} A_h^*}, \quad (21a)$$

$$\text{Maximum-discharge model: } \frac{\tau_n}{\tau_c} = \frac{1}{\alpha_{1D}^{7/3} \max(A_w^*, A_t^*)}. \quad (21b)$$

Equations (21a) and (21b) are useful because they relate the critical shear stress for erosion to the upstream normal-flow bed shear stress, which in turn is related to flood discharge.

3.1. Canyon Formation Regimes

Figure 3 shows an example of how $\frac{\tau_n}{\tau_c}$, given by equations (21a) and (21b), varies with flood Froude number. As Froude number increases, the normalized upstream shear stress required to erode the wall and toe respectively increases and decreases because lateral flow focusing becomes less efficient. Because the normalized upstream shear stress is a function of upstream flow depth, data from Lapotre and Lamb [2015] and the corresponding semiempirical relationships listed in Appendix B can be used to calculate the upstream flow depths that bound canyon formation regimes. When the normalized upstream shear stress of a given flood is smaller than that required to erode the head, no erosion can occur anywhere along the canyon rim. When it is larger than that required to erode the head, but smaller than the

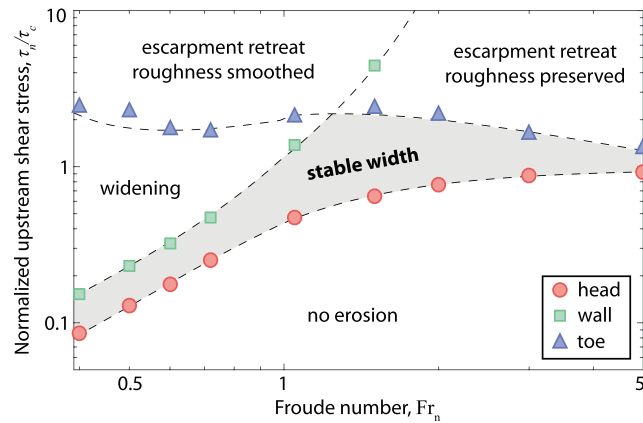


Figure 3. Normalized upstream shear stress (equations (21a) and (21b)) as a function of upstream Froude number, Fr_n , at three locations around the canyon rim (Figure 2)—the head (red circles), the wall (green squares), and the toe (blue triangle; see Figure 2c). This example corresponds to the case of a wide flood ($w^* = 0.1$ and $W^* = 4.5$) flowing over a bed slope, $S = 7.5 \times 10^{-3}$, toward a long canyon ($l^* = 30$), and corresponds to the runs of experiment series 1 of *Lapotre and Lamb* [2015]. Dashed lines result from the semiempirical relationships summarized in Appendix B. Based on the relative values of normalized upstream stress at the canyon head, wall, and toe, we define several canyon-formation regimes. Canyons do not form if the shear stress at the canyon head is less than the critical stress for erosion (“no erosion”). Canyons also do not form for very large normalized shear stresses because erosion is inferred to occur everywhere, including at the canyon toe, leading to the formation of 1-D escarpments that may smooth or preserve the initial topographic roughness of the escarpment. Canyons are predicted to form and lengthen where the shear stress at the canyon head exceeds the threshold for erosion, but the shear stress at the canyon toe does not. If the shear stress at the wall also exceeds the threshold for erosion, then canyons are inferred to widen as they lengthen, whereas stable width canyons have shear stresses that are below the threshold for erosion at the wall.

roughness of the escarpment is preserved, but the roughness does not enlarge to form canyons. Figure 1d is an example of a linear escarpment south of Malad Gorge, Idaho, which may have retreated in one of the latter two regimes.

Widening canyons have increasing canyon-to-flood width ratios, w^* , and decreasing flood-width limitation factors, W^* , and thus have decreasing shear stresses at their walls (Appendix B). Canyon widening can only occur until shear stress at the wall falls below the critical shear stress. At this point, widening stops, and the canyon headwall retreats upstream maintaining a uniform width. A condition for canyon formation while maintaining a uniform width thus is

$$\frac{\tau_n}{\tau_c} \Big|_h \leq \frac{\tau_n}{\tau_c} \leq \left(\frac{\tau_n}{\tau_c} \Big|_w, \frac{\tau_n}{\tau_c} \Big|_t \right). \tag{22}$$

Consequently, $\frac{\tau_n}{\tau_c} \Big|_h$ and $\min\left(\frac{\tau_n}{\tau_c} \Big|_w, \frac{\tau_n}{\tau_c} \Big|_t\right)$, respectively, provide minimum and maximum bounds on the values of the normalized upstream bed shear stress which leads to the formation of a canyon that maintains a uniform width.

3.2. Threshold for Rock Toppling

To constrain the threshold for erosion, τ_c , we assume that waterfall retreat occurs through toppling of rock columns at the rim. Toppling erosion during a flood occurs when the torque exerted by water flow on top of a rock column is large enough to make the column rotate and fail [*Seidl et al., 1996; Lamb and Dietrich, 2009*]. *Lamb and Dietrich* [2009] considered the torque balance on a rock column subjected to shear stress from water flow on top (torque T_s), drag from flow over rock protrusions (T_d), gravity (T_g), and buoyancy

normalized upstream shear stresses required to erode the wall and toe, erosion only occurs around the head, such that the canyon lengthens without widening—our minimum and maximum models are at the bounds of this regime that allows for the formation of canyons with uniform widths (Figures 1a–1c and 1e–1j). Figure 3 illustrates the narrow range in normalized upstream stresses that allow for the formation of a canyon with a uniform width, which implies that canyons with uniform widths evolved under relatively steady flows. Conversely, if the normalized upstream shear stress is greater than that required to erode the walls but lower than that required to erode the toe, the canyon is inferred to both lengthen and widen. Finally, when the normalized upstream shear stress is greater than that required to erode the toe, we distinguish between two regimes in which the entire escarpment retreats. First, if the normalized upstream shear stress is greater than that required to erode the wall, then initial 2-D geometry in the escarpment is smoothed. Second, if the normalized upstream stress is lower than that required to erode the wall, then cliffs with strikes parallel to the main flow direction do not erode, and the initial

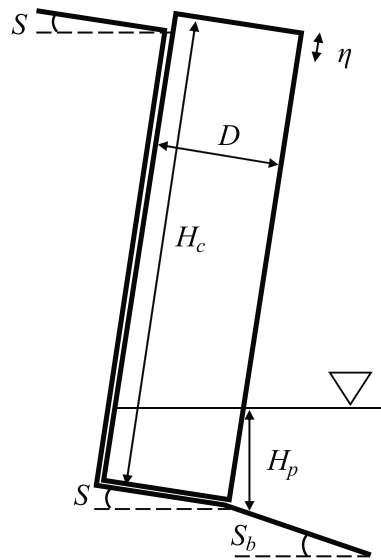


Figure 4. Definition sketch of toppling geometry in side view (adapted from *Lamb and Dietrich [2009]*). A column of width, D , and height, H_c , is partially submerged to a height, H_p , by water in the waterfall plunge pool. The column protrudes over a height, η . Bed slopes upstream and downstream of the overall are denoted S and S_b , respectively.

from a plunge pool (T_b). Toppling of the rock column is predicted when the factor of safety, FS , defined as the ratio of resistive ($T_g - T_b$) to driving ($T_s + T_d$) torques is less than unity. Because the torque associated with bed shear stress at the threshold of failure is $T_s = \tau_c H_c D$, where H_c is the column height and D is the column width (or fracture spacing), one can invert for the threshold bed shear stress accounting for 2-D flow focusing as

$$\tau_c = \frac{1}{2} \left[\rho_r g D \cos \theta \left(1 - \frac{H_c}{D} S \right) - \rho g D \frac{H_p}{H_c} - \rho C_d \frac{\eta}{D} \frac{(\alpha^* \alpha_{1D})^2 h_n^{4/3}}{n^2} \right], \quad (23)$$

where the torques are explicitly written in terms of fracture spacing (D), cliff height (H_c), plunge-pool depth (H_p), column tilt angle ($S = \tan \theta$), protrusion height (η) (Figure 4), water and rock densities (ρ and ρ_r), and a drag coefficient (C_d) over rock protrusions.

3.3. Discharge at the Threshold for Toppling

Finally, to calculate the discharge for canyon formation, the critical shear stress for rock toppling given in equation (23) is substituted into equations (21a) and (21b) to calculate the corresponding normal bed shear stress, τ_n , for the minimum-discharge model (equation (21a)), in which the threshold for toppling is reached at the canyon head, and maximum-discharge

model (equation (21b)), in which the threshold for toppling is reached at the canyon wall or toe. Using these bounds on the normal bed shear stress, the canyon-forming flood discharge into the canyon head is calculated using equation (7) and the relations for the shear stress and discharge enhancement factors, A^* and Q^* , given in Appendices A and B. A^* and Q^* are functions of Fr_n , w^* , W^* , and l^* which can be estimated from the bounds on τ_n and using measurements of canyon geometry, as detailed in section 4. Importantly, the effect of Martian gravity is directly accounted for through equations (7), (21a) and (21b), and (23), and Fr_n . In the next section, we introduce the field sites we chose to apply our new paleohydraulic theory, how the required topographic measurements and observations were performed, and how the inversion procedure was implemented.

4. Field Sites and Methods

4.1. Field Sites

The field sites considered in this study are those shown in Figures 1a–1c and 1e–1j. On Earth, we consider seven canyons in the Snake River Plain of Idaho, (Malad Gorge, North and South; Woody's Cove; Box Canyon; Blind Canyon; Blue Lakes, East and West), six canyons in the Channeled Scablands of Washington (Dry Falls, East and West; Pothole Coulee, North and South; Frenchman Coulee, North and South), and one canyon in Iceland (Ásbyrgi). All of our terrestrial examples are carved into well fractured basaltic flows and were previously suggested to have formed by waterfall retreat. Most of them still have lakes in their heads at the location of past plunge pools, which is further evidence for the existence of waterfalls at the time of carving. All studied terrestrial canyons have flat bottoms and talus slopes downstream of the canyon heads along the sidewalls. These boulders are generally angular and do not show evidence for fluvial transport. In contrast, some boulder bar deposits are observed and show evidence for bedload transport, such as rounding, polishing, and imbrication [e.g., *O'Connor and Baker, 1992; O'Connor, 1993; Lamb et al., 2008, 2014; Baynes et al., 2015a, 2015b*]. Other amphitheater-headed canyons exist, such as Niagara Falls, that are not considered here because they likely form by waterfall plunge-pool erosion processes that differ from the toppling model proposed herein (e.g., see *Lamb et al. [2006]* for discussion).

Table 1. Grain Size and Fracture Spacing Data Compiled at or Near the Studied Canyons^a

Location	Type	D_{16} (m)	D_{50} (m)	D_{84} (m)	Source
Idaho					
BC	grain size	0.13	0.29	0.60	<i>Lamb et al.</i> [2008]
MG	grain size	-	0.58	-	<i>Lamb et al.</i> [2014]
Drumheller, Washington	grain size	0.34	0.59	0.83	this study
As, Iceland	fracture spacing	0.50 (first quartile)	0.65	0.80 (third quartile)	<i>Baynes et al.</i> [2015b]
AV, Mars	grain size	-	4.25 (mean)	-	this study
EC, Mars	fracture spacing	-	4.85 (mean)	-	this study

^aNotations D_{16} , D_{50} , and D_{84} refer to the 16th, 50th, and 84th percentiles of the cumulative grain size distributions, respectively.

The Malad Gorge canyons (MG,N and MG,S, Figure 1a), Woody's Cove (WC, Figure 1a), Box Canyon (BC, Figure 1b), Blind Canyon (BIC, Figure 1b), and the Blue Lakes canyons (BL,E and BL,W, Figure 1c) are all tributaries to the Snake River Canyon in Idaho and are carved within the Snake River Plain, a broad depression filled with volcanic flows erupted between 15 Ma and 2 ka [*Malde*, 1991; *Kauffman et al.*, 2005]. The lava flows hosting the canyons are well jointed, with typical fracture spacings of 30 to 60 cm (Table 1) [e.g., *Lamb and Dietrich*, 2009; *Baynes et al.*, 2015b]. The canyons formed during the Pleistocene Big Lost River, Bonneville, and other floods [e.g., *Malde*, 1960, 1968; *Scott*, 1982; *O'Connor*, 1993; *Rathburn*, 1993; *Lamb et al.*, 2008, 2014].

The Dry Falls canyons (DF,E and DF,W, Figure 1e), Pothole Coulee (PC,N and PC,S, Figure 1f), and Frenchman Coulee canyons (FC,N and FC,S, Figure 1g) are part of the Channeled Scablands, Washington, and were eroded into Miocene basalts [*Mackin*, 1961] by the Missoula floods [e.g., *Bretz*, 1969; *Baker*, 1973; *O'Connor and Baker*, 1992; *Benito and O'Connor*, 2003]. The basaltic flows in the Channeled Scablands are typically well jointed, with a characteristic fracture spacing similar to the measured size of toppled blocks (~60 cm; Table 1). The Channeled Scablands were cut from multiple episodes of catastrophic erosion [*Bretz*, 1969; *Baker*, 1973; *O'Connor and Baker*, 1992; *Benito and O'Connor*, 2003].

Ásbyrgi canyon was carved into basaltic lava flows (<0.8 Ma) [*Johannesson*, 2014] during a glacial outburst flood about 10 ka related to the Jökulsá á Fjöllum river in Iceland [e.g., *Tomasson*, 2002; *Alho et al.*, 2005; *Carrivick et al.*, 2013; *Baynes et al.*, 2015a, 2015b]. Typical joint spacings in the fractured lava flows hosting the canyon are of 50 to 80 cm (Table 1) [*Baynes et al.*, 2015b].

On Mars, we consider two canyon heads along a tributary to the main Ares Vallis outflow channel (Ares Vallis, East and West) and seven canyons along the western rim of Echus Chasma (Echus Chasma, 1–7), the source region of the Kasei Valles outflow-channel system. Martian canyon geometries have likely been modified by the accumulation of debris talus and infilling by subsequent lavas and dust during the several billion years since they were carved, and original canyon bed geometry is not observable at either Ares Vallis or Echus Chasma. While there is no certitude that the Martian canyons considered here formed from rock toppling, or even from waterfall retreat, there is evidence in support of this hypothesis: (1) the lithology is cliff forming, typical of columnar basalt that is prone to toppling [*Lamb and Dietrich*, 2009], (2) scoured channels clearly outline areas of overland flow upstream of the canyon heads (Figure 5a and 5b), and (3) the two sets of Martian canyons are located in the direct vicinity of the two largest outflow channels on the planet. We thus suggest that toppling of jointed basalt by floods is a plausible erosion mechanism at these locations.

The cataract of Ares Vallis (AV,E and AV, W, Figures 1i and 5a) was carved by the Ares Vallis outflow [e.g., *Warner et al.*, 2010]. Several boulder deposits are found downstream of the cataract, and the largest boulders are between 3 and 5.5 m in intermediate diameter (Figure 5c). The Ares Vallis cataract we consider is within a tributary to the main channel considered by *Komatsu and Baker* [1997] and despite being previously studied [e.g., *Pacifici et al.*, 2009; *Warner et al.*, 2010] has not yet been subjected to a paleohydraulic reconstruction.

Canyons at Echus Chasma (EC1–EC7, Figure 1j) are located in the source region of the Kasei Valles outflow channel, east of the Tharsis volcanoes, and were cut into Hesperian fractured volcanics and younger Hesperian volcanic flows [*Rotto and Tanaka*, 1995]. Further evidence for capping lava flows can be observed immediately north of the study area, where lava flows from Tharsis spill over the topographic step of the chasma (e.g., 51°6'31.06"N, 80°14'42.51"W). Figure 5b shows the location of two sample exposures of layers in the walls of EC5 and EC6 (defined in Figure 1j). Figures 5d and 5e show clear layers at these locations,

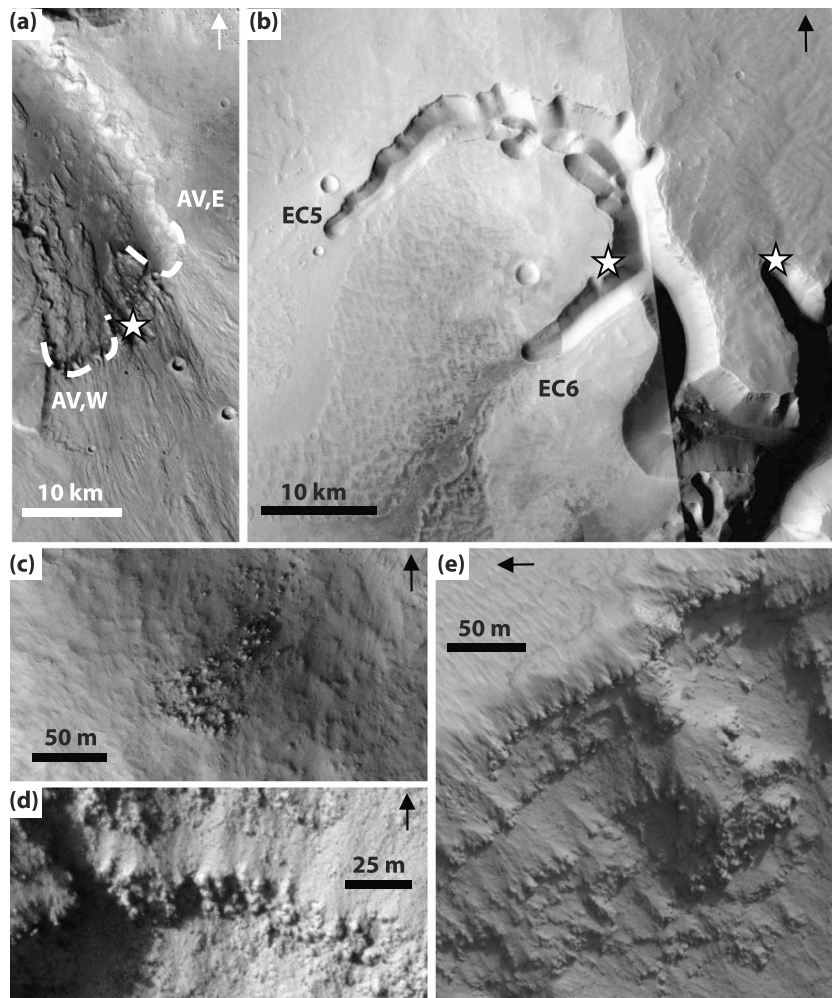


Figure 5. (a) CTX mosaic at the Ares Vallis cataract. The cataract is made of two broad canyon heads (dashed lines). The star indicates the location of Figure 5c. (b) CTX mosaic centered on Echus Chasma canyons EC5 and EC6. The westernmost star indicates the location of Figure 5d, while the easternmost star indicates the location of Figure 5e. (c) HiRISE image PSP_00.538_1885 showing a boulder deposit within the Ares Vallis cataract. Largest boulder sizes are between 3 and 5.5 m. Arrows are indicating the north direction. (d) HiRISE image PSP_009513_1810 (50 cm/pixel) showing layering in the canyon walls and a typical vertical joint spacing of 4.1 to 5.1 m. (e) HiRISE image PSP_009869_1810 (25 cm/pixel) showing layering and rock columns with a vertical joint spacing of 4.5 to 5.6 m.

likely competent lava flows, and potential rock columns that are 4.1 to 5.6 m wide. *Mangold et al.* [2004] showed evidence for overland flow upstream of these canyons (e.g., Figure 5b). *Harrison and Grimm* [2005] argue that waterfall erosion and groundwater sapping may have occurred simultaneously at Echus Chasma. Analogously to the Channel Scablands, the formation of outflow channels on Mars is believed to have required numerous floods to transmit the large inferred water volumes from the subsurface [*Harrison and Grimm*, 2008].

4.2. Field Measurement Methods

Table 2 summarizes topographic measurements for each investigated canyon. All terrestrial topographic measurements are made from Advanced Spaceborne Thermal Emission and Reflection Radiometer (ASTER) digital elevation models (DEMs), except at Ásbyrgi, for which we use data from *Baynes et al.* [2015b]. On Mars, upstream bed slope, S , canyon length, l , and flood width, W , are calculated from Mars Orbiter Laser Altimeter (MOLA) topography, while cliff height, H_c , canyon width, w , and downstream bed slopes, S_b , are measured from Mars Reconnaissance Orbiter (MRO) Context Camera (CTX)-derived DEMs at Echus Chasma [*Shean et al.*, 2011]. All slopes are determined from linear fits to the topographic

Table 2. Values of Topographic/Geometric/Toppling Parameters Used for the Various Canyons^a

	Upstream Bed Slope, S	Downstream Bed Slope, S_b	Canyon Width, w (m)	Canyon Length, l (m)	Flood Width, W (m)	Cliff Height, H_c (m)
<i>Idaho</i>						
MG,N	0.0053	0.029	198	2,245	30,000	64
MG,S	0.0053	0.021	219	2,763	30,000	57
WC	0.0047	0.041	200	387	30,000	63
BC	0.0055	0.044	135	1,768	30,000	37
BIC	0.0047	0.029	168	1,066	30,000	74
BL,E	0.0037	0.043	563	1,200	30,000	93
BL,W	0.0037	0.034	312	516	30,000	74
<i>Washington</i>						
DF,W	9.3×10^{-5}	0.0037	953	2,245	6,000	63
DF,E	9.3×10^{-5}	0.0037	505	2,300	6,000	101
PC,N	3.0×10^{-4}	0.0021	1,468	2,826	3,000	113
PC,S	3.0×10^{-4}	0.0021	762	2,803	3,000	102
FC,N	5.4×10^{-4}	0.0036	546	2,813	7,000	103
FC,S	5.4×10^{-4}	0.0028	627	1,385	7,000	106
<i>Iceland</i>						
As	0.002	0.002	415	3,825	1,325	90
<i>Ares Vallis</i>						
AV,W	0.0044	0.010	5,000	51,200	70,000	280
AV,E	0.0044	0.011	3,500	51,200	70,000	400
<i>Echus Chasma</i>						
EC1	0.0016	0.0029	2,254	30,500	25,000	991
EC2	0.0039	0.0116	2,443	9,500	34,000	900
EC3	0.0037	0.0074	2,480	20,400	34,000	551
EC4	0.0024	0.0075	2,100	7,500	50,000	640
EC5	0.0024	0.0070	1,600	17,000	8,000	440
EC6	0.0032	0.0070	2,876	516	5,000	800
EC7	0.0031	0.0214	2,288	11,000	17,000	1,035

^aAbbreviations used for the different locations are those shown in Figure 1.

data (e.g., Figure 6a), while canyon-head widths are measured by fitting a circle to the headwall (e.g., Figure 6b). The possibility of subsequent widening of the canyons, for example, through glacial and/or mass wasting processes, leads to a possible overestimate of canyon width. Moreover, late-stage infilling of canyons by debris, dust, and/or lava flows may introduce error in downstream bed slope measurements. We thus measured canyon-headwall width within the canyon head as opposed to using cross sections along the sidewalls to minimize the effect of subsequent canyon widening. Moreover, the downstream bed slope averaged over the canyon length should be roughly parallel to that measured along original canyon centerlines provided that infilling rates are uniform along the canyon length. In the toppling model, column tilt angle is here assumed to be equal to the arctangent of S . Flood width, W , is estimated from the top width of channel-like topographic depressions upstream of the canyons. Note that w , l , and W need not be measured with great accuracy because their exact value does not significantly influence results within the observed dimensionless parameter ranges [Lapotre and Lamb, 2015]. Indeed, upstream Froude number has the strongest effect on flow focusing and thus on the distribution of shear stresses along the canyon rim. Upstream Froude number is a function of upstream bed slope, which is measured accurately at the regional scale from ASTER and MOLA topographic data.

Compiled fracture spacing and grain size data are summarized in Table 1. For the canyons in Idaho, we use a fracture spacing of 50 cm to be consistent with Lamb and Dietrich [2009]. In all other locations where only fracture spacings or grain sizes were measured, we assume that $d = D$.

A basaltic density is assumed for rocks on both planets ($\rho_r = 2800 \text{ kg/m}^3$), and the density of water is taken to be $\rho = 1000 \text{ kg/m}^3$. A constant protrusion height to block size ratio is assumed equal to $\eta/D = 0.1$, and the form drag coefficient on rock protrusions is assumed to be $C_d = 1$ [Lamb and Dietrich, 2009; Baynes et al., 2015b]. Bed roughness, k , is calculated from fracture spacing and grain size (i.e., $k = \eta = 0.1D$ upstream of the waterfall

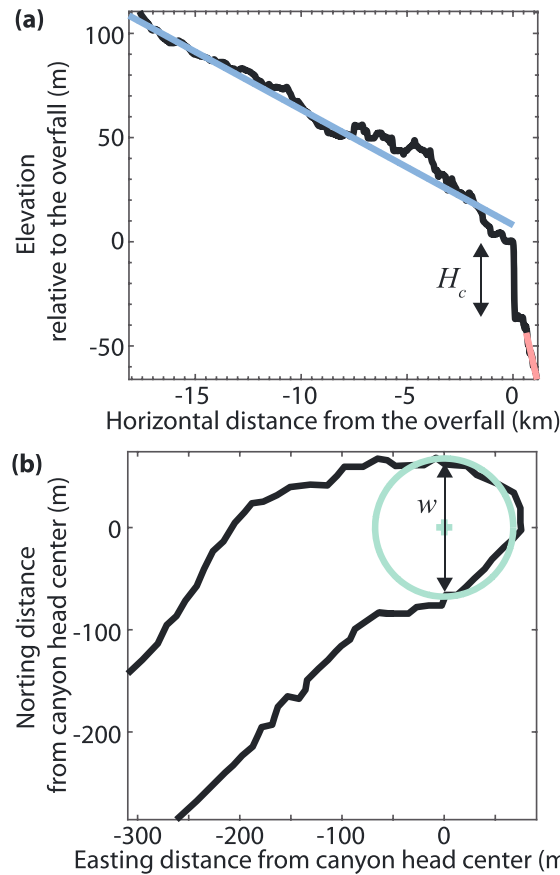


Figure 6. Example of topographic measurements for Box Canyon, Idaho. (a) Long profile showing topography (black), with corresponding linear fits to the upstream bed slope, S (blue), and the downstream bed slope, S_b (red). (b) Map view of delineated canyon headwall (black) and corresponding circle fit to the head (green) performed to measure headwall width, w .

substituted into equations (21a) and (21b) to calculate normal bed shear stress for the minimum-discharge and maximum-discharge models, respectively. Input parameters Fr_n , w^* , W^* , and f^* are calculated from topographic measurements and the constraints on normal bed shear stress and are used to calculate Q^* and A^* from Appendices A and B. Because the constraints on normal bed shear stress require estimates of A^* (equations (21a) and (21b)), and A^* in turn is a function of normal bed shear stress (Appendices A and B), an iterative procedure is used. Finally, normal bed shear stress is substituted into equation (7) to obtain flood discharge into the canyon head. Table 3 summarizes the values of dimensionless parameters that result from the paleohydraulic inversions using the minimum-discharge and maximum-discharge models. Most inverted values fall within the parameter space that was investigated by *Lapotre and Lamb* [2015] and thus in which the fitted relationships used to calculate shear stresses (Appendix B) are most valid.

5. Results

5.1. Discharges, Total Flood Durations, and Water Volumes

Figure 7a shows how our tightest estimated range of flow discharges within the head compares with those inferred from incipient motion and brimful conditions. Table 4 also summarizes head discharges we obtain for the minimum-discharge and maximum-discharge models. Because all of the estimated discharges are lower than the brimful estimate, even for the maximum-discharge model, the tightest estimate range is bounded by $\max(Q_i, Q_{h,\min})$ and $Q_{h,\max}$, where Q_i is calculated from equation (18) and $Q_{h,\min}$ and $Q_{h,\max}$

and $k = 2.5d$ downstream to take into account alluviated eroded material) [*Kamphuis*, 1974; *Lamb and Dietrich*, 2009], and Manning's n is calculated from bed roughness through

$$n \approx \frac{k^{1/6}}{8.1\sqrt{g}}. \quad (24)$$

[*Brownlie*, 1983]. Calculated Manning's n values range from 0.025 to 0.066. Acceleration of gravity was set to 9.81 m/s^2 on Earth and 3.78 m/s^2 on Mars. Finally, the volumetric water-to-rock ratio we use to compare corresponding total flood durations to those estimated from the maximum-discharge model is $\delta = 4.6$. This corresponds to a basaltic sediment mixing ratio of 0.4 by weight, which is typical of hyperconcentrated flows in arid environments on Earth [*Komar*, 1980], and somewhat more reasonable than the maximum observed sediment mixing ratio of 0.65 by weight (i.e., 0.4 by volume), which was used in several studies [e.g., *Carr*, 1996; *Leask et al.*, 2007]. While *Craddock and Howard* [2002] argue that in the case of indurated rock, water-to-rock ratios required for erosion and transport are significantly larger, from 10^4 to 10^5 , we use the 0.4 by weight value to illustrate the endmember sediment hyperconcentration.

4.3. Solution Procedure

To solve for the canyon-forming water discharge, the critical shear stress for toppling is calculated from field or orbital measurements using equation (23), which is substituted

Table 3. Values of Inverted Dimensionless Flow Focusing Parameters for the Minimum-Discharge and Maximum-Discharge Models for the Various Canyons^a

	Upstream Froude Number, Fr_n		Canyon-to-Flood Width Ratio, w^*	Flood Width Limitation Factor, W^*		Downslope Backwater Parameter, f^*	
	Minimum	Maximum		Minimum	Maximum	Minimum	Maximum
<i>Idaho</i>							
MG,N	1.07	1.20	0.01	43.1	22.8	6.5	3.4
MG,S	1.11	1.23	0.01	35.8	19.1	6.6	3.5
WC	1.06	1.15	0.01	28.9	18.0	0.8	0.5
BC	1.19	1.29	0.005	26.9	16.6	3.2	2.0
BIC	1.01	1.13	0.01	38.3	20.2	2.7	1.4
BL,E	0.92	0.90	0.02	25.9	28.4	2.1	2.3
BL,W	0.97	0.96	0.01	18.8	20.1	0.7	0.7
<i>Washington</i>							
DF,W	0.2	0.24	0.16	0.01	0.004	0.01	0.004
DF,E	0.2	0.25	0.08	0.01	0.004	0.01	0.003
PC,N	0.35	0.45	0.49	0.02	0.004	0.1	0.01
PC,S	0.35	0.43	0.25	0.02	0.01	0.1	0.02
FC,N	0.45	0.56	0.08	0.2	0.04	0.1	0.04
FC,S	0.45	0.56	0.09	0.2	0.04	0.1	0.02
<i>Iceland</i>							
As	0.79	0.99	0.31	0.1	0.03	1.1	0.3
<i>Ares Vallis</i>							
AV,W	1.11	1.4	0.07	4.4	1.1	6.9	1.7
AV,E	1.08	1.38	0.05	5.1	1.2	7.9	1.9
<i>Echus Chasma</i>							
EC1	0.71	0.91	0.09	0.3	0.1	0.9	0.2
EC2	0.92	1.14	0.07	3.4	1.0	2.1	0.6
EC3	1	1.25	0.07	1.7	0.5	2.2	0.6
EC4	0.85	1.02	0.04	1.3	0.4	0.4	0.1
EC5	0.87	1.03	0.2	0.1	0.1	0.8	0.3
EC6	0.91	1.13	0.58	0.1	0.03	0.1	0.02
EC7	0.86	1.03	0.13	1	0.3	1.5	0.5

^aAbbreviations used for the different locations are those shown in Figure 1.

correspond to the head discharges inverted from the minimum-discharge and maximum-discharge models, respectively, through equations (7) and (21a) and (21b). On both Earth and Mars, flood discharges into the canyon heads as estimated from the minimum-discharge and maximum-discharge models are in cases more than 2 orders of magnitude smaller than those resulting from the brimful assumption (Figure 7a). Inverted ranges in discharges are consistent across canyons for any given geographic area and are overall higher on Mars ($\sim 10^5\text{--}10^8\text{ m}^3/\text{s}$) than on Earth ($\sim 10^3\text{--}10^6\text{ m}^3/\text{s}$). Discharges at Ásbyrgi are similar to those associated to the Missoula floods ($\sim 10^5\text{--}10^6\text{ m}^3/\text{s}$) and are generally higher than those associated to the Bonneville floods ($\sim 10^3\text{--}10^4\text{ m}^3/\text{s}$).

Figure 7b shows the inverted total flood durations using the maximum-discharge model with the transport-limited assumption (large filled symbols), the brimful and transport-limited assumptions (large open symbols), and the brimful and water-to-rock ratio assumptions (small filled symbols). Note that flood duration cannot be estimated from the minimum-discharge model in many cases because the corresponding discharge is lower than that required for incipient motion. All canyons seem to have formed very rapidly, in a few days to a few months, assuming continuous flow. Mean canyon formation times are 18 days in Idaho, 23 days in Washington, about 4 months for Ásbyrgi, 28 days at Ares Vallis, and 54 days in Echus Chasma. Variations in flooding duration within a given region, for example, at Malad Gorge and Woody's Cove, mostly arise from the significant difference in canyon lengths, which may reflect that the flood branched upstream of the canyon heads and that different flood reaches were active at different times, possibly due to focusing and capture of flood waters by a larger adjacent canyon, as argued by

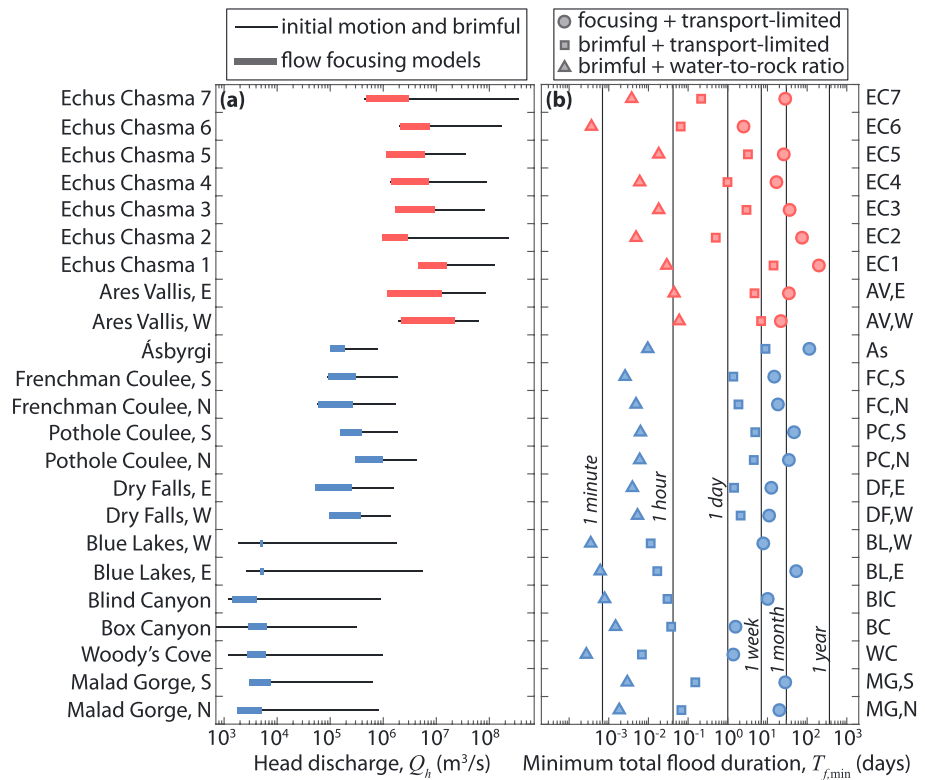


Figure 7. (a) Total flood discharge to the canyon head, Q_h . Thin horizontal lines represent the range bounded by the discharge at initial motion of the observed block sizes (left) and the discharge in brimful conditions (right), while thick horizontal bars are bounded by the smaller of the incipient motion and the minimum-discharge model (left) and the maximum-discharge model (right). Incipient motion estimates are based on measured boulder sizes or fracture spacings (Table 1). (b) Inverted minimum flood duration, $T_{f,min}$, for all considered canyons assuming continuous flow. Large filled symbols correspond to durations inverted from the maximum-discharge model combined to the transport-limited assumption, large open symbols correspond to brimful and transport-limited models, and small filled symbols correspond to brimful and water-to-rock ratio models. Blue and red symbols indicate terrestrial and Martian canyons, respectively.

Lamb et al. [2014]. Note that corresponding total flood durations estimated under the brimful and transport-limited assumptions are shorter by a factor 3 to 3000, with canyon formation lasting from about 10 min to about 2 weeks only. Combining brimful and a water-to-rock ratio assumptions yields even shorter total flood durations, from less than a minute to about an hour. This latter result strongly argues against the hyperconcentration hypothesis. Consistent with the more reasonable volumetric water-to-rock ratios suggested by Craddock and Howard [2002], a water-to-rock ratio of 5×10^4 yields total flood duration that is very similar to those we estimate from the maximum-discharge model and more typical of fluvial bedrock incision on Earth [e.g., Lamb et al., 2015].

Because minimum total flood durations (Figure 7b) calculated from the maximum-discharge model (large circles) are shorter than those calculated assuming brimful conditions (small squares), the total water volumes are similar for both the maximum-discharge ($V_{2D,max}$) and brimful (V_{br}) models, with $V_{br}/V_{2D,max}$ ranging from ~45% to ~90%. Consequently, despite our lowered discharge estimates, the catastrophic floods that carved the amphitheater canyons herein still involved large volumes of water.

5.2. Relationship Between Flow Depths, Discharges, and Canyon Width

Our maximum-discharge toppling model constrains flow depths in the canyons, h_{nb} , to be consistently lower than brimful. Figure 8a shows the derived flow depths in the canyon relative to cliff height as a function of canyon widths. Symbols represent intracanyon depths derived from averaging of the minimum and maximum normal flow depths, while the tips of the vertical bars represent results from the minimum

Table 4. Values of Inverted Flow Depths, Discharges per Unit Width, and Total Head Discharges for the Minimum-Discharge and Maximum-Discharge Models for the Various Canyons^a

	Normal Flow Depth (m)		Normal Discharge per Unit Width (m ² /s)		Total Head Discharge (× 10 ⁴ m ³ /s)	
	<i>h_{n,min}</i>	<i>h_{n,max}</i>	<i>q_{n,min}</i>	<i>q_{n,max}</i>	<i>Q_{h,min}</i>	<i>Q_{h,max}</i>
<i>Idaho</i>						
MG,N	2	2	8	24	0.2	0.5
MG,S	2	4	11	32	0.3	0.8
WC	2	4	13	28	0.3	0.6
BC	3	5	20	44	0.3	0.6
BIC	2	3	8	23	0.1	0.4
BL,E	2	2	9	8	0.5	0.5
BL,W	3	3	15	14	0.5	0.5
<i>Washington</i>						
DF,W	19	56	52	320	6.4	38.4
DF,E	19	63	52	390	3.5	25.6
PC,N	14	59	54	637	8.6	95.2
PC,S	14	50	54	474	4.8	39.3
FC,N	11	39	53	427	3.6	26.2
FC,S	11	39	53	427	4.1	29.9
<i>Iceland</i>						
As	7	27	43	448	1.8	18.6
<i>Ares Vallis</i>						
AV,W	33	136	404	4323	216.6	2244.3
AV,E	28	121	320	3549	120.6	1292.7
<i>Echus Chasma</i>						
EC1	52	245	517	6836	135.8	1561.4
EC2	18	63	136	1105	37.9	288.3
EC3	34	128	391	3513	106.0	918.3
EC4	45	136	502	3123	127.3	714.2
EC5	52	144	633	3447	102.0	599.5
EC6	30	107	288	2431	83.0	748.0
EC7	23	71	178	1200	46.7	297.9

^aAbbreviations used for the different locations are those shown in Figure 1.

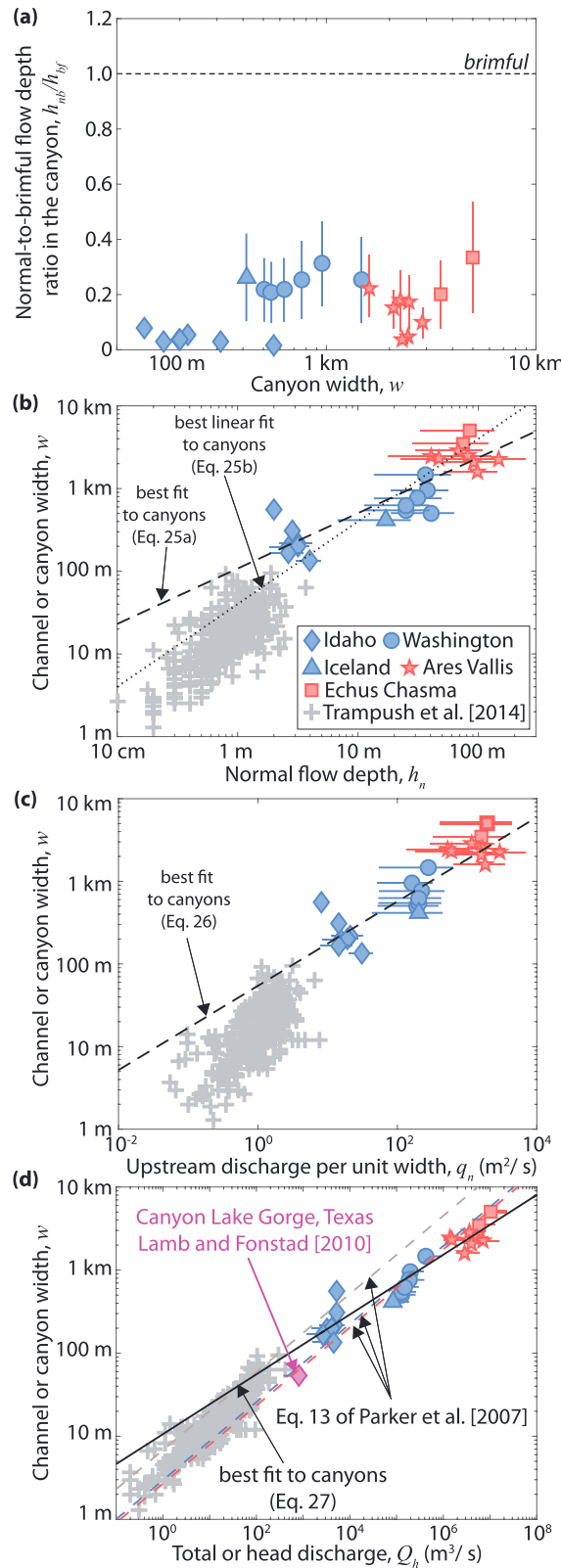
(lower tip) and maximum (upper tip) models. There is no correlation with canyon width, and intracanyon-to-brimful flow depth ratios vary between 2% and 33%. Thus, the toppling model allows for the likely scenario that the water surface drops below the canyon rim during progressive canyon incision, unlike the brimful hypothesis which requires the water surface to maintain its elevation to the canyon rim height throughout canyon formation. All intracanyon flow depths, *h_{nb}*, inverted using the maximum-discharge model are greater than that required for incipient motion of the observed grain sizes, *h_i*. Nevertheless, some of the intracanyon flow depths inverted using the minimum-discharge model are lower than the required flow depth for incipient motion. This result further emphasizes the relative ease with which floods can topple rock columns and that the limiting factor in eroding the canyons is likely the transport of eroded material outside of the canyon head [e.g., Lamb and Fonstad, 2010; Lamb et al., 2015].

Table 4 summarizes inverted normal flow depths upstream of the canyons, discharges per unit width, and total head discharges from the minimum-discharge and maximum-discharge models. Figure 8b shows that there is a positive correlation between the normal flow depth obtained from averaging the minimum-discharge and maximum-discharge models and canyon width (dashed line),

$$w \approx 107.8h_n^{0.67}, (R^2 = 0.77). \tag{25a}$$

Symbols represent the average of the minimum and maximum normal flow depths, while the tips of the bars represent results from the minimum (left tip) and maximum (right tip) models. A linear fit instead provides a useful, order-of-magnitude approximation to equation (25a) (dotted line),

$$w \approx 40h_n, (R^2 = 0.58). \tag{25b}$$



There also exists a positive correlation between canyon width, w , and upstream discharge per unit width, q_n (Figure 8c). The best fit relationship between normal flow discharge per unit width and canyon width is

$$w = 54.4 q_n^{0.51}, \quad (R^2 = 0.80). \quad (26)$$

Equation (26) can be used as a forward predictor of the width of canyons eroded by a flood of a given discharge. While there is an inevitable correlation between volumetric discharge to the canyon head and canyon width from mass conservation, it need not be the case for upstream discharge per unit width, and the existence of such a correlation supports our hypothesis that the width of canyons carved by floods is set in part by flood discharge. The best fit relationship between total head discharge and canyon width (Figure 8d) is

$$w = 10.6 Q_h^{0.36}, \quad (R^2 = 0.91). \quad (27)$$

Our findings yield $Q_h/q_n = aw^b$, where $a \approx 3.6$, which is consistently greater than unity due to flow focusing, and $b \approx 0.82$, which is consistently close to unity, due to the inevitable correlation arising from mass conservation. In

Figure 8. (a) Inverted normal-to-brimful flow depths ratio, h_{nb}/h_{br} , in the canyons as a function of canyon headwall width (blue and red symbols indicate terrestrial and Martian canyons, respectively). (b) Canyon width as a function of inverted normal flow depth for all considered canyons, compared with channel widths and depths of coarse-grained rivers on Earth (gray crosses) [Trampush et al., 2014]. Bars represent the range bounded by the minimum (left tip) and maximum (right tip) models, while the symbols are derived from an upstream normal flow depth that is the average of $h_{n,min}$ and $h_{n,max}$, the normal flow depths obtained from the minimum-discharge and maximum-discharge models, respectively. (c) Canyon width as a function of upstream normal discharge per unit width, compared with gravel bed rivers on Earth (gray crosses) [Trampush et al., 2014]. (d) Canyon width as a function of head discharge for all considered canyons, compared with gravel bed rivers on Earth (gray crosses) [Trampush et al., 2014], predictions for gravel bed rivers (dashed lines) [Parker et al., 2007], and a modern canyon erosion event at Canyon Lake Gorge, Texas (magenta diamond) [Lamb and Fongstad, 2010]. The continuous black line represents the best fit power law given in equation (27), and the gray, blue, and red dashed lines are predictions from Parker et al. [2007], for $d = 4 \text{ mm}$ and $g = 9.81 \text{ m/s}^2$, $d = 60 \text{ cm}$ and $g = 9.81 \text{ m/s}^2$, and $d = 4 \text{ m}$ and $g = 3.78 \text{ m/s}^2$, respectively.

Table 5. Summary of Values Used for Sensitivity Analysis

	Canyon Width, w (m)	Flood Width, W (m)	Bed Slope, S	Cliff Height, H_c (m)	Fracture Spacing, D (m)
Bed slope	150	2000	10^{-5} – 10^{-2}	80	0.5
Fracture spacing	150	2000	10^{-3}	80	0.1–10

section 6.3, we discuss how these relationships between width, depth, and discharge compare to those observed in coarse-grained rivers on Earth [e.g., Parker *et al.*, 2007].

6. Discussion

6.1. Sensitivity Analysis of Discharge Predictions

Our flow-focusing model is most sensitive to upstream bed slope, S (in that it sets the value of upstream Froude number, Fr_n), and canyon-to-flood width ratio, w^* , when upstream Froude number is relatively low [Lapotre and Lamb, 2015]. Moreover, the toppling model is most sensitive to column tilt angle and fracture spacing, D [Lamb and Dietrich, 2009]. For the canyons herein considered, focusing does not seem to have been strongly influenced by confinement (high w^* at low Fr_n , Table 3). We thus illustrate the sensitivity of our model to upstream bed slope, S , and fracture spacing, D . In the following modeling exercise, acceleration of gravity was set to 9.81 m/s^2 rock and water density to 2800 and 1000 kg/m^3 , respectively. The same values of protrusion height to block size ratio, h/D , form drag coefficient over rock protrusions, C_d , and bed roughness parametrization as for the case studies were used in the sensitivity analysis. Canyon length was set to 5 km.

Parameter values used to model the effect of bed slope, S , on rock toppling and flow focusing are summarized in Table 5 for subcritical to supercritical floods ($Fr_n \approx 0.1 - 1.25$, $w^* \approx 0.08$, $W^* \approx 3 \times 10^{-4} - 5$, and $I^* \approx 10^{-3} - 30$). Figures 9a–9c show how bed slope upstream of the waterfall affects inverted flow depth and cumulative head discharge. When slope is small, I^* is small; i.e., A_t^* is large. Up to a value of $S \approx 8 \times 10^{-5}$, $A_t^* > A_w^*$ decreases (Figure 9a), leading to higher flow depths and head discharges (Figures 9b and 9c). For $8 \times 10^{-5} \leq S \leq 2 \times 10^{-3}$, $A_w^* > A_t^*$ decreases due to an increasing upstream Froude number, Fr_n (Figure 9a). Overall, increasing bed slope leads to lower critical shear stress for toppling and smaller flood depths. This effect dominates when flow becomes critical at around $S \approx 2 \times 10^{-3}$, which leads to a decrease in normalized upstream stress. At $S \approx 5 \times 10^{-3}$, rock columns become gravitationally unstable; i.e., no water is required for toppling to occur (Figure 9b). Bedrock canyons considered in this study have slopes ranging between 10^{-4} and 5×10^{-3} . Within this range, flow focusing is set by A_w^* , which is relatively insensitive to bed slope, S (Figure 9a). Flow focusing is most sensitive to bed slope when $A_t^* > A_w^*$, i.e., when I^* is small. Consequently, the Channeled Scablands canyons likely are the most sensitive to errors in bed slope measurements. For example, using the maximum-discharge model, underestimating a slope of 10^{-4} by 50% (i.e., $S = 5 \times 10^{-5}$) leads to a head discharge underestimated by 18%, while a 50% overestimate of the slope (i.e., $S = 2 \times 10^{-4}$) produces little error (<1%).

Parameter values used to model the effect of fracture spacing on rock toppling and flow focusing are summarized in Table 5 for a subcritical flood ($Fr_n \approx 0.1 - 0.75$, $w^* \approx 0.08$, $W^* \approx 10^{-2} - 1$, and $I^* \approx 6 \times 10^{-2} - 5$). Figures 9d–9f illustrate how fracture spacing, D , affects both rock toppling and flow focusing for a subcritical flood. When fracture spacing increases, larger normal flow depths are required to topple rock columns (Figure 9e). This effect causes the flood-width limitation factor, W^* , to decrease and drop below unity because the lateral backwater length becomes larger than half of the flooded width, and flow focusing becomes limited by the size of the flood. Consequently, the shear stress enhancement factor at the wall, A_w^* , also decreases (Figure 9d). The increase in normalized upstream stress leads to higher discharges needed to form a horseshoe canyon (Figure 9f). Note that the minimum-discharge model becomes brimful at $D \approx 6.5 \text{ m}$, while the maximum-discharge model becomes brimful at $D \approx 1.5 \text{ m}$. With the maximum-discharge model, underestimating a fracture spacing of 50 cm by 50% ($D \approx 25 \text{ cm}$) leads to an underestimate in head discharge of 71%, while a 50% overestimate of fracture spacing ($D \approx 1 \text{ m}$) causes the head discharge to be overestimated by 160%. Inverted normal flow depth and head discharge scale roughly linearly with fracture

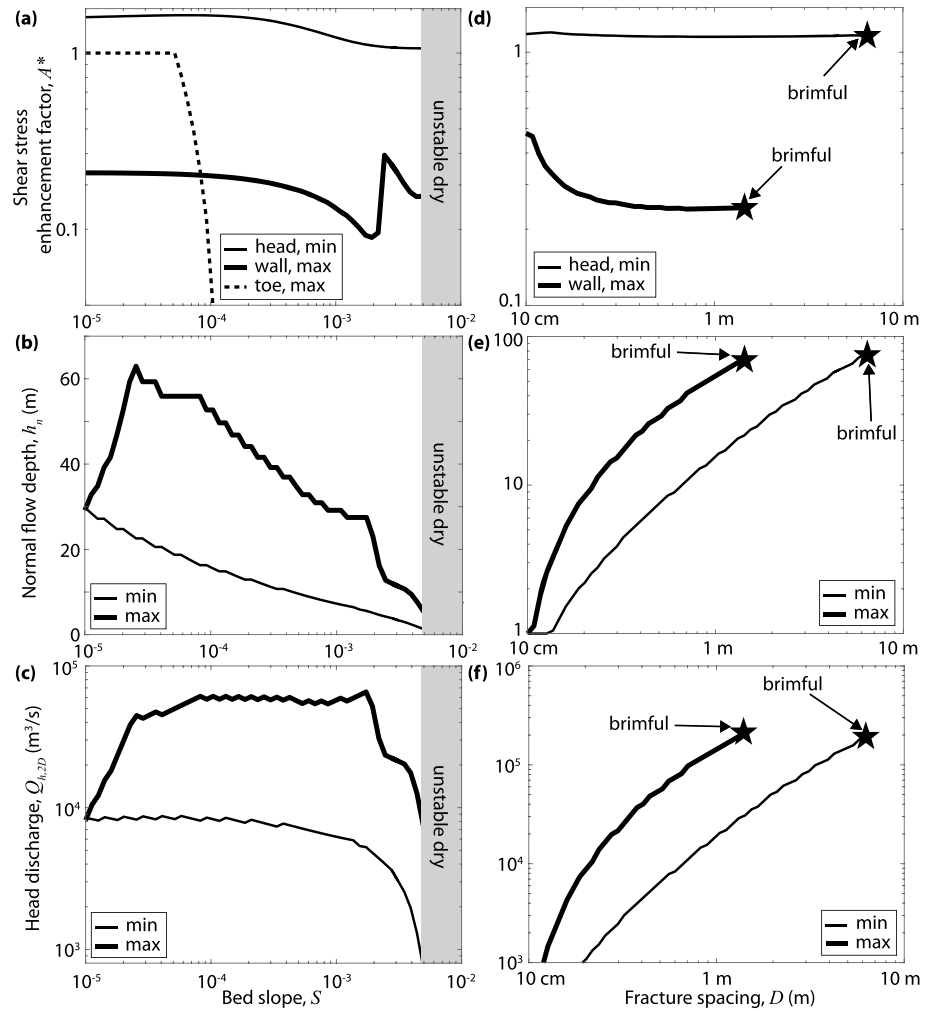


Figure 9. Sensitivity analysis. (a, d) Shear stress enhancement factor, A^* ; (b, e) normal flow depth, h_n ; and (c, f) cumulative head discharge, $Q_{h,2D}$, as a function of bed slope, S , and fracture spacing, D , respectively. Shaded areas correspond to zones of gravitationally unstable rock-column slope. Parameter values used here are summarized in Table 5.

spacing, and the error introduced by erroneous fracture spacings is unlikely to produce order-of-magnitude uncertainty in flow depth and discharge.

6.2. Comparison to Previous Work for Case Studies

O'Connor [1993] estimated peak discharges of the Bonneville flood based on the elevation of high water marks and step-backwater flow modeling to approximately $10^6 m^3/s$, and flood duration was estimated to about 100 days. In the Eden channel near Twin Falls, Idaho, where the two Blue Lakes canyons are located, he estimated a peak discharge of $0.57 \times 10^6 - 0.62 \times 10^6 m^3/s$. Our average estimate of minimum total flood duration of about 30 days is lower than that of O'Connor [1993]. The sum of our cumulative discharges into the head of both Blue Lakes canyons, which are located within the Eden channel, is approximately 1.0×10^4 to $1.1 \times 10^4 m^3/s$, which is consistently lower than estimates from O'Connor [1993]. These differences occur because (1) the Blue Lakes canyons only represent a portion of the total width of the Eden channel and (2) estimates from high water marks provide an upper bound on flow discharge given that they may represent a flow stage associated to previous channel geometries that were subsequently further incised. At Box Canyon, Lamb et al. [2008] estimated that flood discharge was greater than $200 m^3/s$ based on observed block sizes, constrained normal discharge per unit width, q_n , to be greater than $3.2 - 11.2 m^2/s$ from the geometry of a channel upstream of the canyon head which overspilled, and estimated flood duration to about 35 to 160 days. We calculate a minimum total flood duration of

about 1.6 days and an upstream discharge per unit width of about 20 to 44 m²/s, which are consistently lower and larger than the estimates of *Lamb et al.* [2008], respectively. This outcome makes sense because their estimate is a true minimum. At Malad Gorge, *Lamb et al.* [2014] estimated that flow discharge had to be greater than 1.25×10^3 m³/s in order to transport the observed block sizes out of the canyon heads. We estimate discharges of 2×10^3 to 5×10^3 and 3×10^3 to 8×10^3 m³/s in the heads of the north and south canyons at Malad Gorge, respectively, which again is consistent with the true minimum discharges calculated by *Lamb et al.* [2014].

Peak discharges associated to the Missoula floods are typically thought to be $>10^7$ m³/s as estimated from high water marks and 1-D flow hydraulics [e.g., *Baker, 1973; O'Connor and Baker, 1992; Amidon and Clark, 2014*]. Based on discharges estimated from the brimful assumption, *Baker* [1973] estimated that it took a maximum of 14 h to pond water from Lake Missoula and overspill at the Wallula Gap, and associated waning flows would have lasted for 1 to 2 weeks. Downstream of the Dry Falls canyons, near Soap Lake, water discharge was estimated to be about 4.5×10^6 m³/s based on the location of high water marks and assuming that current channels were brimful to the level of the high water marks [*Baker, 1973*]. We estimate a total water discharge required to carve the canyons at Dry Falls, Pothole Coulee, and Frenchman Coulee to be about 3.2×10^5 to 2.55×10^6 m³/s, and a minimum total flood duration of about 23 days, which are consistently smaller flow magnitude and longer duration than the discharge and flood duration estimated by *Baker* [1973], respectively. This difference arises because our reconstruction puts flow stage at less than brimful. The sum of our two Dry Falls head discharges is approximately 9.9×10^4 to 6.4×10^5 m³/s, which is smaller than the discharge estimate by *Baker* [1973] near Soap Lake, suggesting again that high water marks may have been deposited at an early flood stage and do not represent peak flow within the modern-day topography.

At Ásbyrgi canyon, *Baynes et al.* [2015a] estimated that the minimum discharge required to initiate transport of the observed block sizes as bedload is 3.9×10^4 m³/s. Based on the toppling model of *Lamb and Dietrich* [2009], *Baynes et al.* [2015b] calculated the minimum discharge required to topple basalt columns at Selfoss, about 25 km upstream of Ásbyrgi, to be greater than 3.25×10^3 m³/s. Other paleohydraulic approaches including flow routing over present-day topography have estimated the largest flood discharges along the Jökulsá á Fjöllum to be approximately 0.9×10^6 m³/s [e.g., *Alho et al., 2005; Carrivick et al., 2013*]. At Ásbyrgi, we constrain the discharge to be between 1.8×10^4 and 1.9×10^5 m³/s, which is consistent with the lower bound estimates from *Baynes et al.* [2015a, 2015b] and consistently lower than brimful conditions over present-day topography. *Baynes et al.* [2015a] proposed that Ásbyrgi formed in a single flood event based on the lack of evidence for diffusion of the cliff face over time. Nevertheless, our minimum total flood duration of about 4 months is longer than that of typical glacial outburst floods in Iceland [*Bjornsson, 2003*] and may represent the summed duration of multiple flood events instead.

In the main Ares Vallis channel, *Komatsu and Baker* [1997] estimated a flood discharge of 10^8 – 10^9 m³/s assuming brimful flow conditions, while *Andrews-Hanna and Phillips* [2007] estimate a total discharge of 10^6 – 10^7 m³/s for the source region of the outflow channel near Iani Chaos by modeling the outburst of an overpressurized underground aquifer. We estimate that the discharge required to carve the Ares Vallis cat-act is of about 3.4×10^6 to 3.5×10^8 m³/s, which overlaps with discharges estimated by *Andrews-Hanna and Phillips* [2007] and the lower end of the range estimated by *Komatsu and Baker* [1997].

Echus Chasma is the source region for the Kasei Valles outflow-channels system. *Robinson and Tanaka* [1990] estimated a total discharge of 1×10^9 – 2.3×10^9 m³/s from the brimful assumption in Kasei Valles, while *Williams et al.* [2000] estimated lower discharges by constraining channel geometry from the elevation of fluvial terraces near the outlet of the outflow to Chryse Planitia of about 8×10^4 to 2×10^7 m³/s, and *Kleinhaus* [2005] estimated a larger discharge of 3.7×10^9 m³/s using a different implementation for bed friction. Summing up our minimum-discharge and maximum-discharge models for the seven investigated canyons of Echus Chasma yields a total discharge of 6.4×10^6 to 5.1×10^7 m³/s, which is consistently lower than the brimful estimates and is similar to the discharges obtained by *Williams et al.* [2000] for the Northern Kasei Valles route but higher than their Southern Kasei Valles route estimate. The relatively high value of our discharges compared with those of *Williams et al.* [2000] might arise because we calculate discharge near the source region at the canyon head, while they focused on terraces near the outlet of the channels to Chryse Planitia.

6.3. Controls on Canyon Morphology

Our model applies to canyon formation in lithologies that are prone to waterfall erosion by rock toppling, such as columnar basalt, such that canyons tend to evolve to a state set by the threshold for erosion. Importantly, flow focusing toward a canyon head is found to be relatively weak such that there exists only a narrow region of parameter space in which flood-induced shear stresses exceed a threshold for erosion at the canyon head while simultaneously falling below the erosion threshold along the canyon walls (Figure 3). It is these conditions that we infer lead to the formation of a canyon, through upstream canyon-head retreat, of uniform width. Thus, long canyons of uniform width contain useful and tightly constrained bounds on the minimum and maximum canyon-forming discharges (Figure 3). Our model also implies that flood discharges were relatively steady during canyon formation, at least where canyon width appears to have been uniform during canyon-headwall retreat. Similar to Figure 2, our threshold model implies that feedbacks should exist that drive canyon widening or narrowing until an equilibrium width is established for a certain flood discharge. For example, bed shear stress will be large along the walls of an undersized canyon, which should lead to toppling along the canyon sidewalls and widening. For an even larger flood event, the model predicts that waterfalls retreat as linear escarpments (e.g., Figure 1d) if flood discharges are too high to produce bed shear stresses below the critical value for erosion along the sidewalls of an embayment (Figure 3). Thus, canyons that widen upstream and eroded linear escarpments indicate floods with shear stresses that greatly exceed the critical stress for erosion (Figure 3) or floods with increasing discharge in time and thus imply larger paleodischarges or unsteady flow as compared with uniform width canyons. A lower bound on the flood discharge responsible for the retreat of linear escarpments can be calculated from the maximum-discharge model. Conversely, canyons that narrow upstream may preserve information about the falling limb of flood discharge.

In the case of canyon-forming floods, the existence of a positive correlation between flood discharge per unit width and the width of canyons, over 2 orders of magnitude in canyon width and almost 3 orders of magnitude in discharge on two different planets (Figure 8c), is consistent with our hypothesis that flood discharge in part controls canyon width. Thus, bedrock canyon width represents a powerful paleohydraulic tool to reconstruct the discharge of past outburst floods from readily available datasets. Discharge and canyon width both contribute to setting flow depth within the canyon (equation (15)), which ultimately sets the value of the Shields stress for sediment transport, which itself is a useful parameter to estimate flood discharge based on observations of grain size within a channel (equation (14)). Figure 10 shows the inverted Shields stresses in the canyon heads normalized by the critical Shields stress. Thin lines represent the range bounded by incipient motion ($\tau_* / \tau_{*c} = 1$) and brimful conditions. For some canyons, the minimum-discharge model yields predicted Shields stresses in the head that are lower than that required for incipient motion. Consequently, the tightest lower bound constraint on Shields stress in the head is provided by $\max(h_i, h_{nb,min})$, where $h_{nb,min}$ is the intracanyon depth obtained from the minimum-discharge model. Thick lines represent the range bounded by the tightest lower bound and the maximum-discharge model. We find that the empirical distribution of our tightest range in Shields stress to critical Shields stress ratio has a median of 1.6, for which the 68% confidence interval is 1.4 to 2.1. Inverted Shields stresses are most sensitive to fracture spacing, D , and bottom slopes, S_b . Further uncertainty may arise from the fact that rock columns did not fail over their total height, H_c ; however, inverted discharges are not sensitive to column height as long as $H_c \gg D$. Uncertainty might also arise from the fit relationships (Appendix B), but most dimensionless focusing parameters fall within ranges tested in *Lapotre and Lamb* [2015].

With inverted Shields stresses ranging between 1.4 and 2.1 times the critical value, sediment fluxes within the canyons were relatively low (equation (13)), likely outpaced by the rate of toppling downstream of the canyon head, which supports the hypothesis that erosion was transport-limited, consistent with other theoretical considerations [*Lamb et al.*, 2015] and observations [*Lamb and Fongstad*, 2010]. In comparison, Shields stresses within the head under brimful conditions (upper tip of thin lines in Figure 10) indicate that observed sediment sizes would be transported in suspension in many cases, which is inconsistent with the presence of boulder bar deposits in most of our terrestrial examples that are analogous to the bank-attached expansion bars of *Bretz et al.* [1956] and *Baker* [1973] and typically form from bedload transport in coarse-bedded rivers on Earth [e.g., *Costa*, 1983; *Wohl*, 1992]. Boulder bars could also form during the falling flood limb, but many have widths that are a large fraction of the canyon width, similar to bars in

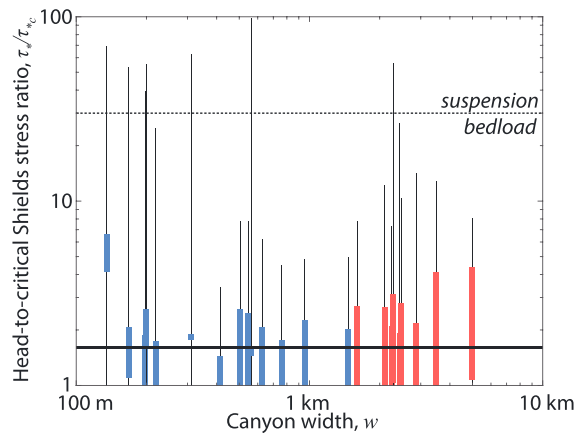


Figure 10. Inverted Shields stress within the canyon heads (τ_s) normalized by the critical Shields stress ($\tau_{*c} \approx 0.045$) as a function of canyon width, w , for all considered canyons. Thin vertical lines represent the range bounded by initial motion (lower tip) and brimful (upper tip) conditions in the canyon. Only the maximum-discharge model values are systematically above unity. Thick vertical lines represent the tightest range of Shields stress to critical Shields stress ratios as determined by either incipient motion or the minimum-discharge model (lower tip) and the maximum-discharge model (upper tip). The continuous line represents the inverted median Shields stress within all canyon heads of $\tau_s \approx 1.6\tau_{*c}$. Dashed line represents the transition between bedload transport and suspension, estimated by equating the flow shear velocity, u_s , to the sediment fall velocity, $v_s = \sqrt{\frac{4}{3} \left(\frac{Rgd}{C_d} \right)}$, and assuming a drag coefficient, C_d , of unity, consistent with large natural boulders [e.g., Ferguson and Church, 2004].

coarse-grained rivers [e.g., Ikeda, 1984; Seminara and Tubino, 1989; Garcia and Nino, 1993], and heights consistent with our estimated intracanyon flow depths, suggesting that they formed in concert with canyon formation.

The fact that we invert for a consistent, low, and finite Shields stress within all canyon heads suggests that there may exist a morphodynamic feedback setting its value. For example, in the case of gravel bed rivers, it was shown that brimful width is set such that grains are transported at the bottom of the channel but are not entrained along the erodible banks (so-called *threshold channel theory*), with Shields stresses along the bed predicted by both theory and modeling to be roughly 1.1 to 1.5 times the critical Shields stress value [Parker, 1978; Kovacs and Parker, 1994; Cao and Knight, 1997; Vigilar and Diplas, 1997, 1998]. This range overlaps with the range of Shields stresses we found for the 14 terrestrial and nine Martian canyons.

We suggest that in toppling terrain, the finite low range in Shields stresses results from (1) the similarity between the toppling threshold and the critical stress for incipient motion [e.g., Lamb and Fonstad, 2010; Lamb et al., 2014, 2015] and (2) the relatively narrow range in rim shear stresses relative to the critical value that leads to the formation of canyons with uniform widths (section 3). Indeed, the sizes of the transported blocks in the canyon are similar to rock column width, and the critical shear stress for toppling is mostly a function of column width. Bed shear stresses within the canyon head are inevitably close to the value of the shear stresses around the canyon-head rim, which we showed ought to be close to the critical threshold for toppling. Thus, bed shear stresses within the canyon ought to be close to the threshold shear stress for incipient motion, and the range in Shields stresses is dictated by the range of rim stresses that allow for the formation of a canyon with a uniform width. Consequently, the inverted range in intracanyon Shields stresses may serve as a convenient proxy to estimate bounds on flow discharge and duration in toppling terrain. The similarity between intracanyon Shields stress and the critical shear stress for toppling also is consistent with the formation of boulder bars.

If canyons form at a near-threshold state, similar to gravel bed rivers, we might expect a similarity in the hydraulic geometries of gravel bed rivers and toppling-dominated canyons. This expectation contrasts with abrasion-dominated slot canyons, which have lower erosion rates than toppling-dominated canyons, and lower width-to-depth ratios than gravel bed rivers [e.g., Carter and Anderson, 2006]. In Figure 8b, we compare our bedrock canyons to a compilation of coarse-grained rivers on Earth [Trampush et al., 2014] and find that they appear to have similar width-to-depth ratios (47^{+36}_{-25} for bedrock canyons and 18^{+15}_{-7} for coarse-grained rivers, where the $+/-$ values represent the 68% confidence interval of the width-to-depth ratio). Figure 8d shows that the width of bedrock canyons correlates positively with head discharge and that this correlation is very similar to that observed in gravel bed rivers on Earth [Trampush et al., 2014] and at a modern example of a flood-carved canyon: Canyon Lake Gorge, Texas [Lamb and Fonstad, 2010]. Canyon Lake Gorge is one of the few modern examples of an entire canyon forming by plucking-dominated waterfall erosion during a megaflood. Many other waterfalls exist on Earth, but most

erode slowly through plunge-pool abrasion during more normal floods [e.g., Crosby and Whipple, 2006; Lamb et al., 2007; DiBiase et al., 2015], rather than block toppling during megafloods that is our focus here. The width-discharge relationship we infer for megaflood-carved canyons seems to be well predicted by semiempirical theory for gravel bed rivers from Parker et al. [2007]. In the case of toppling-dominated canyons, our model suggests that flood width and Froude number may play an important role in that they affect flow focusing and thus the length scale over which shear stresses drop below the critical value for toppling. Nevertheless, the apparent universality of equation (27) likely arises from (1) the relative insensitivity of flow focusing on flood width when $w \ll W$, (2) the fact that floods typically have Froude numbers close to unity [e.g., Costa, 1987; Grant, 1997; Tinkler, 1997; Richardson and Carling, 2006], (3) relatively uniform block sizes on a given planetary body, and (4) the fact that some parameters covary, e.g., larger block sizes in a lower gravity field on Mars, possibly offsetting their relative effects on toppling mechanics.

6.4. Implications for Water on Mars

Individual Martian outburst floods might have provided sufficient water to, at least transiently, enable the existence of a northern ocean [e.g., Parker et al., 1989; Baker et al., 1991], which, depending on its volume and stability, could have altered the Martian global climate [e.g., Baker, 2002]. Although our estimated discharges are much lower than previously thought, corresponding water volumes remain large. For example, estimated volumes to carve the two canyons at Ares Vallis and the seven canyons at Echus Chasma are about $8.0 \times 10^{13} \text{ m}^3$ and $3.5 \times 10^{14} \text{ m}^3$, respectively, or about 2–10% of the volume of the Mediterranean Sea. A water volume of 10^{14} m^3 delivered at once to the Martian surface corresponds to a 70 cm thick global equivalent layer (GEL). If concentrated to the northern lowlands (about one third of the Martian surface), such a water volume would create a >2 m deep body of water. Conversely, if it was derived from a 33% porous global aquifer, the water outflow would perturb the global aquifer over a thickness of >2 m.

Although early Mars is thought to have hosted large volumes of water (a more than 137 m GEL [Villanueva et al., 2015]), remote and in situ D/H isotopic measurements show that the global water inventory decreased rapidly throughout the Noachian, and the measured total volume of water reservoirs on present-day Mars corresponds to a 20–30 m GEL [e.g., Lasue et al., 2013]. These estimated volumes encompass all known reservoirs in the surface and shallow subsurface. A ~137 m GEL, which likely is a conservative upper bound for the late Noachian-early Hesperian transition, is equivalent to the volume of ~200 floods (based on individual flood volumes of 10^{14} m^3). Thus, despite their lowered discharges, Martian floods still constitute a significant fraction of the total water budget of the planet, and their outburst from the subsurface to the surface likely altered the global hydrology of Mars.

The source of catastrophic flood water is the subject of an active debate, but it is generally thought to result from pressurization of underground aquifers [Carr, 1979; Burr et al., 2002; Chapman and Tanaka, 2002; Manga, 2004; Hanna and Phillips, 2006; Wang et al., 2006; Meresse et al., 2008; Burr, 2010; Zegers et al., 2010; Marra et al., 2014a, 2014b]. Because water discharge transmitted by a porous aquifer is proportional to the medium's permeability, our lowered discharge estimates may help in resolving a long-standing paradox: if the surface water that formed the Martian outflow channels indeed emanated from the ground, Martian regolith would be required to have the permeability of loose gravel to transmit the discharges inferred from the brimful assumption [e.g., Wilson et al., 2004; Pelletier and Baker, 2011]. However, a 2-orders-of-magnitude decrease in water discharge, as suggested by our modeling, translates into required aquifer permeabilities that are 2 orders of magnitude lower, i.e., similar to those of moderately fractured rocks [Bear, 1972].

Finally, despite lowered discharges and thus longer time-integrated flood durations, Martian outburst floods remain short-lived, consistent with a catastrophic origin of the flood waters. Our revised durations, of up to two months, are on the higher end of typical durations for individual modern terrestrial glacial floods [e.g., Bjornsson, 2003], and these relatively long durations are consistent with the possibility that multiple flood events are responsible for the formation of the Martian canyons, as has been inferred by others from observations of terraces and inner channels [e.g., Harrison and Grimm, 2008; Pacifici et al., 2009; Warner et al., 2009]. However, it is unclear whether a subsurface pressurization mechanism would be able to trigger episodic floods [e.g., Manga, 2004; Wang et al., 2006].

7. Conclusion

Some canyons carved in fractured basaltic flows on Earth and Mars likely formed through waterfall retreat. Because of the crystalline and fractured nature of basaltic bedrock, toppling of rock columns under the action of water flow at the canyon head is a good candidate mechanism for waterfall retreat. We developed a new theory for canyon dynamics that takes into account the distribution of bed shear stresses imparted by flood water along the rim of amphitheater-headed canyons. We propose that canyons with a spatially uniform width must evolve such that flow focusing allows for erosion of the canyon head but not along the canyon sidewalls. Because flow focusing is, in general, limited, our model implies that canyons form under conditions very close to the threshold for erosion. Thus, all else being equal, larger floods should produce wider canyons. We applied this new paleohydraulic method to 14 terrestrial (Malad Gorge, Woody's Cove, Box Canyon, Blind Canyon, Blue Lakes canyons in Idaho, Dry Falls, Pothole Coulee, Frenchman Coulee in Washington, and the Ásbyrgi canyon in Iceland) and nine Martian (Echus Chasma and Ares Vallis) canyons and found a relationship between the formative discharge of floods and the headwall width of the canyons they carved, consistent with our hypothesis. We showed that the predicted discharges of those floods were in cases more than 2 orders of magnitude lower than previous estimates assuming brimful conditions. Under the assumption that canyon erosion was transport-limited, we showed that canyon formation typically lasted from less than a day to a few months, although these times may have been proportioned into shorter discrete flood events. We derived formative Shields stresses for sediment transport within the canyon heads and found that they were within 1.4 to 2.1 times the critical value for incipient motion of the observed block sizes, which likely arises from the relatively narrow range in rim shear stresses that allow for a stable-width canyon, and the similarity between toppling and initial motion thresholds. Consequently, this range in Shields stresses may constitute a convenient closure to place bounds on flood discharge and duration in toppling terrain. Finally, we predicted that despite their lowered discharges, the considered floods involved similar volumes of water compared with their corresponding brimful estimates. In particular, estimated water volumes suggest that the floods required to carve the observed canyons were large enough to have significantly perturbed the subsurface and surface hydrology of Mars at a global scale.

Appendix A: Acceleration Factor Ratio and Normalized Cumulative Discharge Fit Relationships From Lapotre and Lamb [2015]

The acceleration factor ratio at the head, α_h^* , decreases with Froude number, Fr_n , for subcritical floods and is roughly equal to unity for supercritical floods.

$$\alpha_h^* = \begin{cases} 1 + 0.05(1 - Fr_n)^{1.65} & \text{for } Fr_n < 1 \\ 1 & \text{for } Fr_n \geq 1 \end{cases} \quad (\text{A1})$$

In the case of a sheet flood ($w^* \ll 1$ and $W^* > 1$), the acceleration factor ratio at the wall, α_w^* , decreases with Froude number, Fr_n , and the decrease is steeper for Fr_n between 1 and 3.

$$\alpha_{w,sf}^* = 1.47 \exp \left[- \left(\frac{Fr_n + 1.18}{1.58} \right)^2 \right] - 0.53 \exp \left[- \left(\frac{Fr_n + 0.03}{0.53} \right)^2 \right] + 85550 \exp \left[- \left(\frac{Fr_n + 51}{14.7} \right)^2 \right]. \quad (\text{A2})$$

For a sheet flood, the acceleration factor ratio at the toe, α_t^* , increases with Froude number, Fr_n , and decreases with the downslope backwater parameter, l^* .

$$\alpha_{t,sf}^* = \begin{cases} (2.08Fr_n^{0.11} - 1.76)(3.68l^{*-0.31}) & \text{for } Fr_n < 1 \\ (2.08Fr_n^{0.11} - 1.76)(2.02 - 0.29l^{*0.35}) & \text{for } Fr_n \geq 1 \end{cases} \quad (\text{A3})$$

For subcritical nonsheet floods, the acceleration factor at the wall, α_w^* , decreases with the canyon-width to flood-width ratio, w^* , and increases with the flood-width limitation factor, W^* (as long as $W^* < 1$). For supercritical nonsheet floods, the acceleration factor ratio at the wall, α_w^* , slightly increases with canyon-width to flood-width ratio, w^* .

$$\alpha_w^* = \begin{cases} \alpha_{w,sf}^*(1 - w^*)^{0.22} G_1 & \text{for } Fr_n < 1 \\ \alpha_{w,sf}^*(5.80w^{*0.06} - 4.07) & \text{for } Fr_n \geq 1 \end{cases} \quad (\text{A4})$$

in which

$$G_1 = \begin{cases} [1.06 - 0.38(1 - W^*)^{1.41}] & \text{for } W^* < 1 \\ [1.07 - 7.72 \times 10^{-3}W^*] & \text{for } W^* \geq 1 \end{cases} \quad (A5)$$

The acceleration factor ratio at the toe, α_t^* , for subcritical nonsheet floods increases with w^* and decreases with W^* . For supercritical nonsheet floods, the acceleration factor ratio at the toe, α_t^* , increases with both w^* and W^* .

$$\alpha_t^* = \begin{cases} \alpha_{t,sf}^* (0.87 - 21.75w^{*4.65}) [1.18 \exp(0.01W^*) - 1.39 \exp(-0.38W^*)] & \text{for } Fr_n < 1 \\ \alpha_{t,sf}^* (1 + 0.68w^{*5.09}) [1.07 - 1.21 \exp(-0.49W^*)] & \text{for } Fr_n \geq 1 \end{cases} \quad (A6)$$

Normalized cumulative head discharge, Q^* , decreases with Froude number, Fr_n , increases and then decreases with flood-width limitation factor, W^* , and either decreases or is constant with canyon-width to flood-width ratio, w^* , depending on whether the flood is subcritical or supercritical.

$$Q^* = \begin{cases} [1 + 0.79 \exp(-2.16Fr_n)] (1.14 - 0.33w^{*0.37}) G_2 & \text{for } Fr_n < 1 \\ [1 + 0.79 \exp(-2.16Fr_n)] & \text{for } Fr_n \geq 1 \end{cases} \quad (A7)$$

where

$$G_2 = \begin{cases} [1.03 - 0.16(1 - W^*)^{2.85}] & \text{for } W^* < 1 \\ [1.08 - 0.04W^{*0.31}] & \text{for } W^* \geq 1 \end{cases}$$

Note that these fit relationships are valid for the tested range and combinations of dimensionless parameters listed in *Lapotre and Lamb* [2015] but should be used with caution when applied near the edges of the modeled parameter ranges modeled for nonsheet floods. They were tested against test simulations that encompassed different parameter combinations and are yet to be validated outside of the modeled ranges. Nevertheless, most of the acceleration factor ratios have predictable asymptotical behaviors.

Appendix B: Shear Stress Enhancement Factor

Fit relationships for the shear stress enhancement factors were obtained from the numerical simulations of *Lapotre and Lamb* [2015] through multiple power law regressions, following the technique described in the latter study. All trends are qualitatively similar to those observed for the acceleration factor ratios, α^* , and are discussed at length in *Lapotre and Lamb* [2015].

Shear stress enhancement factor at the head, A_h^* :

$$A_h^* = 0.37 \exp \left[- \left(\frac{Fr_n - 0.17}{0.38} \right)^2 \right] + 1.04 \exp \left[- \left(\frac{Fr_n - 2.89}{78.6} \right)^2 \right]. \quad (B1)$$

Shear stress enhancement factor at the wall, A_w^* :

$$A_w^* = 0.79 \exp \left[- \left(\frac{Fr_n - 6.68 \times 10^{-2}}{1.13} \right)^2 \right] G_3, \quad (B2)$$

where

$$G_3 = \begin{cases} (1 - w^*)^{0.38} G_4 & \text{for } Fr_n < 1 \\ 1 & \text{for } Fr_n \geq 1 \end{cases} \quad (B3)$$

and

$$G_4 = \begin{cases} [0.76 - 0.32(1 - W^*)^{1.44}] & \text{for } W^* < 1 \\ [1.03 - 0.27W^{*-2.62}] & \text{for } W^* \geq 1 \end{cases} \quad (B4)$$

Shear stress enhancement factor at the toe, A_t^* :

$$A_t^* = (0.47Fr_n^{0.47} - 0.26)G_5, \quad (B5)$$

where

$$G_5 = \begin{cases} (0.79 - 8.24w^{*3.39})(0.47W^{*0.58} - 0.26)(8.38l^{*-0.49}) & \text{for } Fr_n < 1 \\ (1 + 0.96w^{*3.46})(1.13W^{*0.37} - 0.87)(2.84 - 0.51l^{*0.31}) & \text{for } Fr_n \geq 1 \end{cases}. \quad (B6)$$

Notations

- A_c canyon cross-sectional area (m^2).
- A^* shear stress enhancement factor at the waterfall brink.
- A_c^* normalized critical shear stress for rock toppling.
- A_h^* shear stress enhancement factor at the canyon head.
- A_t^* shear stress enhancement factor at the canyon toe.
- A_w^* shear stress enhancement factor at the canyon wall.
- C_d drag coefficient over rock protrusions.
- C_f dimensionless bed friction coefficient.
- C_{f0} dimensionless bed friction coefficient at the waterfall brink.
- d grain diameter (m).
- D fracture spacing/block size (m).
- Fr_n upstream Froude number.
- FS toppling factor of safety.
- g acceleration of gravity (m/s^2).
- h flow depth (m).
- h_{bf} flow depth in brimful conditions (m).
- h_i flow depth at initiation of sediment motion (m).
- h_n normal flow depth upstream of the waterfall (m).
- h_{nb} normal flow depth within the canyon (m).
- h_0 flow depth at the waterfall brink (m).
- H_c cliff/rock column height (m).
- H_p plunge pool depth (m).
- k bed roughness (m).
- l canyon length (m).
- l^* downslope backwater factor.
- n Manning's n .
- q_i discharge per unit width at initiation of sediment motion (m^2/s).
- q_n upstream discharge per unit width (m^2/s).
- q_{sc} sediment capacity per unit width (m^2/s).
- $Q_{h,2D}$ discharge within the canyon head as inverted from the 2-D model (m^3/s).
- Q_{sc} Sediment capacity (m^3/s).
- Q^* normalized cumulative head discharge.
- R reduced density of sediment.
- S upstream bed slope.
- S_b bed slope within the canyon.
- T_b torque per unit width exerted by buoyancy on a rock column (N).
- T_d torque per unit width exerted by flow drag on a rock column (N).
- T_f total flood duration (s).
- T_g torque per unit width exerted by gravity on a rock column (N).
- T_s torque per unit width exerted by flow shear on a rock column (N).
- U_n upstream flow velocity (m/s).
- U_0 flow velocity at the waterfall brink (m/s).

w	canyon width (m).
w^*	canyon-to-flood-width ratio.
W	flood width (m).
W^*	flood-width limitation factor.
α	acceleration factor at the brink of a waterfall.
α^*	acceleration factor ratio.
α_{1D}	acceleration factor at the brink of a 1-D step.
α_{2D}	acceleration factor at the brink of a 2-D canyon.
γ	canyon cross-sectional geometry shape factor.
δ	volumetric water-to-rock ratio.
η	column protrusion height (m).
ρ	density of water (kg/m^3).
ρ_r	density of rock (kg/m^3).
τ_c	critical shear stress for rock toppling (N/m^2).
τ_0	shear stress exerted by flow at the waterfall brink (N/m^2).
$\tau_{0,1D}$	shear stress exerted by flow at the brink of a 1-D step (N/m^2).
$\tau_{0,2D}$	shear stress exerted by flow at the brink of a 2-D canyon (N/m^2).
τ_*	Shields stress for initiation of sediment motion.
τ_{*c}	critical Shields stress for initiation of sediment motion.

Acknowledgments

The authors are grateful to Liliya Posiolova of Malin Space Science Systems for assistance with CTX DEM generation and the students of Ge121a at Caltech for sharing grain size data collected within the Drumheller channel, Washington, in the fall of 2013. We also thank Paul Carling and an anonymous reviewer for their constructive comments which improved this manuscript. Support was provided by the NASA Earth and Space Science Fellowship 12-PLANET12F-0071, NSF grants EAR-1147381 and 1529110, and NASA grant NNX13AM83G. Derived data are available in appendices and tables.

References

- Alho, P., A. J. Russell, J. L. Carrivick, and J. Kayhko (2005), Reconstruction of the largest Holocene jokulhlaup within Jokulsa A Fjollum, NE Iceland, *Quat. Sci. Rev.*, 24(22), 2319–2334, doi:10.1016/j.quascirev.2004.11.021.
- Amidon, W. H., and A. C. Clark (2014), Interaction of outburst floods with basaltic aquifers on the Snake River Plain: Implications for Martian canyons, *Geol. Soc. Am. Bull.*, 127(5–6), 688–701, doi:10.1130/B31141.1.
- Andrews-Hanna, J. C., and R. J. Phillips (2007), Hydrological modeling of outflow channels and chaos regions on Mars, *J. Geophys. Res.*, 112, E08001, doi:10.1029/2006JE002881.
- Baker, V. (2002), High-energy megafloods: Planetary settings and sedimentary dynamics, in *Flood and Megaflood Processes and Deposits: Recent and Ancient Examples, Spec. Publ.*, vol. 32, edited by I. P. Martini, V. R. Baker, and G. Garzon, pp. 3–15, Int. Assoc. of Sedimentol., Malden, Mass.
- Baker, V., and D. J. Milton (1974), Erosion by catastrophic floods on Mars and Earth, *Icarus*, 23(1), 27–41.
- Baker, V., R. Strom, V. Gulick, J. Kargel, G. Komatsu, and V. Kale (1991), Ancient oceans, ice sheets and the hydrological cycle on Mars, *Nature*, 352, 589–594, doi:10.1038/352589a0.
- Baker, V. R. (1973), *Paleohydrology and Sedimentology of Lake Missoula Flooding in Eastern Washington*, *Geol. Soc. Am. Spec. Pap.*, vol. 144, pp. 1–73.
- Baynes, E. R., M. Attal, A. J. Dugmore, L. A. Kirstein, and K. A. Whaler (2015a), Catastrophic impact of extreme flood events on the morphology and evolution of the lower Jokulsa a Fjollum (northeast Iceland) during the Holocene, *Geomorphology*, 250, 422–436.
- Baynes, E. R. C., M. Attal, S. Niedermann, L. A. Kirstein, A. J. Dugmore, and M. Naylor (2015b), Erosion during extreme flood events dominates Holocene canyon evolution in northeast Iceland, *Proc. Natl. Acad. Sci. U.S.A.*, 112(8), 2355–2360, doi:10.1073/pnas.1415443112.
- Bear, J. (1972), *Dynamics of Fluids in Porous Media*, 764 pp., Elsevier, New York.
- Benito, G., and J. E. O'Connor (2003), Number and size of last-glacial Missoula floods in the Columbia River valley between the Pasco Basin, Washington, and Portland, Oregon, *Geol. Soc. Am. Bull.*, 115(5), 624–638, doi:10.1130/0016.
- Bibring, J.-P., Y. Langevin, A. Gendrin, B. Gondet, F. Poulet, M. Berthe, A. Soufflot, R. Arvidson, N. Mangold, and J. Mustard (2005), Mars surface diversity as revealed by the OMEGA/Mars Express observations, *Science*, 307(5715), 1576–1581, doi:10.1126/science.1108806.
- Bjornsson, H. (2003), Subglacial lakes and jokulhlaups in Iceland, *Global Planet. Change*, 35(3), 255–271, doi:10.1016/S0921-8181(02)00130-3.
- Bollaert, E. (2004), A comprehensive model to evaluate scour formation in plunge pools, *Int. J. Hydropower Dams*, 11(1), 94–101.
- Bresse, J. A. C. (1866), *Cours de Mecanique Appliquee: Hydraulique, Professeur l'Ecole Imperiale des Ponts et Chaussées*, 568 pp., Gauthier-Villars, Paris.
- Bretz, J. H. (1969), The Lake Missoula floods and the channeled scabland, *J. Geol.*, 77(5), 505–543.
- Bretz, J. H., H. U. Smith, and G. E. Neff (1956), Channeled Scabland of Washington: New data and interpretations, *Geol. Soc. Am. Bull.*, 67(8), 957–1049.
- Brownlie, W. R. (1983), Flow depth in sand-bed channels, *J. Hydraul. Eng.*, 109(7), 959–990.
- Burr, D. M. (2010), Palaeoflood-generating mechanisms on Earth, Mars, and Titan, *Global Planet. Change*, 70(1–4), 5–13, doi:10.1016/j.gloplacha.2009.11.003.
- Burr, D. M., J. A. Grier, A. S. McEwen, and L. P. Keszthelyi (2002), Repeated aqueous flooding from the Cerberus Fossae: Evidence for very recently extant, deep groundwater on Mars, *Icarus*, 159(1), 53–73, doi:10.1006/icar.2002.6921.
- Cao, S., and D. W. Knight (1997), Entropy-based design approach of threshold alluvial channels, *J. Hydraul. Res.*, 35(4), 505–524.
- Carr, M. H. (1979), Formation of Martian flood features by release of water from confined aquifers, *J. Geophys. Res.*, 84(NB6), 2995–3007, doi:10.1029/JB084iB06p02995.
- Carr, M. H. (1986), Mars: A water-rich planet?, *Icarus*, 68(2), 187–216.
- Carr, M. H. (1996), *Water on Mars*, 229 pp., Oxford Univ. Press, New York.
- Carr, M. H., and J. W. Head (2010), Geologic history of Mars, *Earth Planet. Sci. Lett.*, 294(3–4), 185–203, doi:10.1016/j.epsl.2009.06.042.

- Carrivick, J. L., F. S. Tweed, P. Carling, P. Alho, P. M. Marren, K. Staines, A. J. Russell, E. L. Rushmer, and R. Duller (2013), Discussion of "Field evidence and hydraulic modeling of a large Holocene jokulhlaup at Jokulsa A Fjollum channel, Iceland" by Douglas Howard, Sheryl Luzzadder-Beach and Timothy Beach, 2012, *Geomorphology*, *201*, 512–519.
- Carter, C. L., and R. S. Anderson (2006), Fluvial erosion of physically modeled abrasion-dominated slot canyons, *Geomorphology*, *81*(1), 89–113, doi:10.1016/j.geomorph.2006.04.006.
- Chapman, M. G., and K. L. Tanaka (2002), Related magma-ice interactions: Possible origins of chasmata, chaos, and surface materials in Xanthe, Margaritifer, and Meridiani Terrae, Mars, *Icarus*, *155*(2), 324–339, doi:10.1006/icar.2001.6735.
- Chatanantavet, P., and G. Parker (2009), Physically based modeling of bedrock incision by abrasion, plucking, and macroabrasion, *J. Geophys. Res.*, *114*, F04018, doi:10.1029/2008JF001044.
- Chow, V. T. (1959), *Open Channel Hydraulics*, 681 pp., McGraw-Hill, New York.
- Christensen, P. R., J. L. Bandfield, M. D. Smith, V. E. Hamilton, and R. N. Clark (2000), Identification of a basaltic component on the Martian surface from Thermal Emission Spectrometer data, *J. Geophys. Res.*, *105*(E4), 9609–9621, doi:10.1029/1999JE001127.
- Coleman, S. E., B. W. Melville, and L. Gore (2003), Fluvial entrainment of protruding fractured rock, *J. Hydraul. Eng.*, *129*(11), 872–884, doi:10.1061/(ASCE)0733-9429(2003)129.
- Costa, J. E. (1983), Paleohydraulic reconstruction of flash-flood peaks from boulder deposits in the Colorado Front Range, *Geol. Soc. Am. Bull.*, *94*(8), 986–1004.
- Costa, J. E. (1987), Hydraulics and basin morphometry of the largest flash floods in the conterminous United States, *J. Hydrol.*, *93*(3), 313–338.
- Craddock, R. A., and A. D. Howard (2002), The case for rainfall on a warm, wet early Mars, *J. Geophys. Res.*, *107*(E11), 5111, doi:10.1029/2001JE001505.
- Crosby, B. T., and K. X. Whipple (2006), Knickpoint initiation and distribution within fluvial networks: 236 waterfalls in the Waipaoa River, North Island, New Zealand, *Geomorphology*, *82*(1), 16–38, doi:10.1016/j.geomorph.2005.08.023.
- de Vries, M. (1965), Consideration about non-steady bed-load transport in open channels, paper presented at 11th Congress Int. Assoc. of Hydraul. Res., Leningrad, USSR, Saint Petersburg, Russia.
- Delleur, J., J. Dooge, and K. Gent (1956), Influence of slope and roughness on the free overfall, *J. Hydraul. Div. Am. Soc. Civ. Eng.*, *82*(4), 1–35.
- DiBiase, R. A., K. X. Whipple, M. P. Lamb, and A. M. Heimsath (2015), The role of waterfalls and knickzones in controlling the style and pace of landscape adjustment in the western San Gabriel Mountains, California, *Geol. Soc. Am. Bull.*, *127*(3–4), 539–559, doi:10.1130/B31113.1.
- Dunne, T. (1990), Hydrology, mechanics, and geomorphic implications of erosion by subsurface flow, in *Groundwater Geomorphology*, *Geol. Soc. Am. Spec. Pap.*, vol. 252, edited by C. G. Higgins and D. R. Coates, pp. 1–28.
- Ehlmann, B. L., and C. S. Edwards (2014), Mineralogy of the Martian surface, *Annu. Rev. Earth Planet. Sci.*, *42*, 291–315, doi:10.1146/annurev-earth-060313-055024.
- Ferguson, R., and M. Church (2004), A simple universal equation for grain settling velocity, *J. Sediment. Res.*, *74*(6), 933–937, doi:10.1306/051204740933.
- Fernandez Luque, R., and R. Van Beek (1976), Erosion and transport of bed-load sediment, *J. Hydraul. Res.*, *14*(2), 127–144.
- Flores-Cervantes, J. H., E. Istanbuluoglu, and R. L. Bras (2006), Development of gullies on the landscape: A model of headcut retreat resulting from plunge pool erosion, *J. Geophys. Res.*, *111*, F01010, doi:10.1029/2004JF000226.
- Garcia, M., and Y. Nino (1993), Dynamics of sediment bars in straight and meandering channels: Experiments on the resonance phenomenon, *J. Hydraul. Res.*, *31*(6), 739–761.
- Gilbert, G. K. (1907), The rate of recession of Niagara Falls, *U.S. Geol. Surv. Bull.*, *306*, 1–31.
- Grant, G. E. (1997), Critical flow constrains flow hydraulics in mobile-bed streams: A new hypothesis, *Water Resour. Res.*, *33*(2), 349–358, doi:10.1029/96WR03134.
- Hager, W. H. (1983), Hydraulics of plane free overfall, *J. Hydraul. Eng.*, *109*(12), 1683–1697.
- Hanna, J. C., and R. J. Phillips (2006), Tectonic pressurization of aquifers in the formation of Mangala and Athabasca Valles, Mars, *J. Geophys. Res.*, *111*, E03003, doi:10.1029/2005JE002546.
- Harrison, K. P., and R. E. Grimm (2005), Groundwater-controlled valley networks and the decline of surface runoff on early Mars, *J. Geophys. Res.*, *110*, E12S16, doi:10.1029/2005JE002455.
- Harrison, K. P., and R. E. Grimm (2008), Multiple flooding events in Martian outflow channels, *J. Geophys. Res.*, *113*, E02002, doi:10.1029/2007JE002951.
- Haviv, I., Y. Enzel, K. Whipple, E. Zilberman, J. Stone, A. Matmon, and L. Fifield (2006), Amplified erosion above waterfalls and oversteepened bedrock reaches, *J. Geophys. Res.*, *111*, F04004, doi:10.1029/2006JF000461.
- Head, J. W., A. L. Nahm, D. R. Marchant, and G. Neukum (2006), Modification of the dichotomy boundary on Mars by Amazonian mid-latitude regional glaciation, *Geophys. Res. Lett.*, *33*, L08S03, doi:10.1029/2005GL024360.
- Howard, A. D. (1994), A detachment-limited model of drainage basin evolution, *Water Resour. Res.*, *30*(7), 2261–2285, doi:10.1029/94WR00757.
- Howard, A. D., and C. F. McLane (1988), Erosion of cohesionless sediment by groundwater seepage, *Water Resour. Res.*, *24*(10), 1659–1674, doi:10.1029/WR024i010p01659.
- Howard, A. D., R. C. Kochel, and H. E. Holt (1987), *Sapping Features of the Colorado Plateau: A Comparative Planetary Geology Field Guide*, *NASA Spec. Publ.*, vol. 491, 118 pp., NASA, Washington, D. C.
- Ikeda, S. (1984), Prediction of alternate bar wavelength and height, *J. Hydraul. Eng.*, *110*(4), 371–386.
- Izumi, N., and G. Parker (1995), Inception of channelization and drainage basin formation: Upstream-driven theory, *J. Fluid Mech.*, *283*, 341–363.
- Izumi, N., and G. Parker (2000), Linear stability analysis of channel inception: Downstream-driven theory, *J. Fluid Mech.*, *419*, 239–262, doi:10.1017/S0022112000001427.
- Johannesson, H. (2014), Geological map of Iceland, in *Bedrock Geology*, 2nd scale 1:600,000 ed., Icelandic Institute of Natural History and Iceland Geodetic Survey, Reykjavik, Iceland.
- Kamphuis, J. (1974), Determination of sand roughness for fixed beds, *J. Hydraul. Res.*, *12*(2), 193–203.
- Kauffman, J., K. Othberg, V. Gillerman, and D. Garwood (2005), *Geologic Map of the Twin Falls 30 × 60 Minute Quadrangle, Idaho*, Idaho Geol. Surv., Moscow, Idaho.
- Kleinhaus, M. (2005), Flow discharge and sediment transport models for estimating a minimum timescale of hydrological activity and channel and delta formation on Mars, *J. Geophys. Res.*, *110*, E12003, doi:10.1029/2005JE002521.
- Komar, P. D. (1980), Modes of sediment transport in channelized water flows with ramifications to the erosion of the Martian outflow channels, *Icarus*, *42*(3), 317–329.

- Komatsu, G., and V. R. Baker (1997), Paleohydrology and flood geomorphology of Ares Vallis, *J. Geophys. Res.*, *102*(E2), 4151–4160, doi:10.1029/96JE02564.
- Kovacs, A., and G. Parker (1994), A new vectorial bedload formulation and its application to the time evolution of straight river channels, *J. Fluid Mech.*, *267*, 153–183.
- Laity, J. E., and M. C. Malin (1985), Sapping processes and the development of theater-headed valley networks on the Colorado Plateau, *Geol. Soc. Am. Bull.*, *96*(2), 203–217.
- Lamb, M. P., and W. E. Dietrich (2009), The persistence of waterfalls in fractured rock, *Geol. Soc. Am. Bull.*, *121*(7–8), 1123–1134, doi:10.1130/b26482.1.
- Lamb, M. P., and M. A. Fonstad (2010), Rapid formation of a modern bedrock canyon by a single flood event, *Nat. Geosci.*, *3*(7), 477–481, doi:10.1038/ngeo894.
- Lamb, M. P., A. D. Howard, J. Johnson, K. X. Whipple, W. E. Dietrich, and J. T. Perron (2006), Can springs cut canyons into rock?, *J. Geophys. Res.*, *111*, E07002, doi:10.1029/2005JE002663.
- Lamb, M. P., A. D. Howard, W. E. Dietrich, and J. T. Perron (2007), Formation of amphitheater-headed valleys by waterfall erosion after large-scale slumping on Hawai'i, *Geol. Soc. Am. Bull.*, *119*(7–8), 805–822.
- Lamb, M. P., W. E. Dietrich, S. M. Aciego, D. J. DePaolo, and M. Manga (2008), Formation of Box Canyon, Idaho, by megaflood: Implications for seepage erosion on Earth and Mars, *Science*, *320*(5879), 1067–1070, doi:10.1126/science.1156630.
- Lamb, M. P., B. H. Mackey, and K. A. Farley (2014), Amphitheater-headed canyons formed by megaflooding at Malad Gorge, Idaho, *Proc. Natl. Acad. Sci. U.S.A.*, *111*(1), 57–62, doi:10.1073/pnas.1312251111.
- Lamb, M. P., N. J. Finnegan, J. S. Scheingross, and L. S. Sklar (2015), New insights into the mechanics of fluvial bedrock erosion through flume experiments and theory, *Geomorphology*, *244*, 33–55, doi:10.1016/j.geomorph.2015.03.003.
- Lapotre, M. G. A., and M. P. Lamb (2015), Hydraulics of floods upstream of horseshoe canyons and waterfalls, *J. Geophys. Res. Earth Surf.*, *120*, 1227–1250, doi:10.1002/2014JF003412.
- Lasue, J., N. Mangold, E. Hauber, S. Clifford, W. Feldman, O. Gasnault, C. Grima, S. Maurice, and O. Mouis (2013), Quantitative assessments of the Martian hydrosphere, *Space Sci. Rev.*, *174*(1–4), 155–212, doi:10.1007/s11214-012-9946-5.
- Leask, H. J., L. Wilson, and K. L. Mitchell (2007), Formation of Mangala Valles outflow channel, Mars: Morphological development and water discharge and duration estimates, *J. Geophys. Res.*, *112*, E08003, doi:10.1029/2006JE002851.
- Luo, W., R. E. Arvidson, M. Sultan, R. Becker, M. K. Crombie, N. Sturchio, and Z. El Alfy (1997), Ground-water sapping processes, western desert, Egypt, *Geol. Soc. Am. Bull.*, *109*(1), 43–62.
- Mackin, J. H. (1961), A stratigraphic section in the Yakima Basalt and the Ellensburg Formation in south-central Washington, Washington Division of Mines and Geology Rep. Inv. 19, 45 pp., Olympia, Wash.
- Malde, H. (1960), Evidence in the Snake River plain, Idaho, of a catastrophic flood from Pleistocene Lake Bonneville, in *Short Papers in the Geological Sciences, U.S. Geol. Surv. Prof. Pap.*, vol. 400, pp. 295–297.
- Malde, H. E. (1968), The catastrophic late Pleistocene Bonneville flood in the Snake River plain, Idaho, *U.S. Geol. Surv. Prof. Pap.* 596, 52.
- Malde, H. E. (1991), Quaternary geology and structural history of the Snake River Plain, Idaho and Oregon, *Geol. North Am.*, *2*, 251–281.
- Manga, M. (2004), Martian floods at Cerberus Fossae can be produced by groundwater discharge, *Geophys. Res. Lett.*, *31*, L02702, doi:10.1029/2003GL018958.
- Mangold, N., C. Quantin, V. Ansan, C. Delacourt, and P. Allemand (2004), Evidence for precipitation on Mars from dendritic valleys in the Valles Marineris area, *Science*, *305*(5680), 78–81.
- Marra, W. A., L. Braat, A. W. Baar, and M. G. Kleinhans (2014a), Valley formation by groundwater seepage, pressurized groundwater outbursts and crater-lake overflow in flume experiments with implications for Mars, *Icarus*, *232*, 97–117, doi:10.1016/j.icarus.2013.12.026.
- Marra, W. A., E. Hauber, S. J. McLelland, B. J. Murphy, D. R. Parsons, S. J. Conway, M. Roda, R. Govers, and M. G. Kleinhans (2014b), Pressurized groundwater outflow experiments and numerical modeling for outflow channels on Mars, *J. Geophys. Res. Planets*, *119*, 2668–2693, doi:10.1002/2014JE004701.
- Mason, P. J., and K. Arumugam (1985), Free jet scour below dams and flip buckets, *J. Hydraul. Eng.*, *111*(2), 220–235.
- McIntyre, N., N. H. Warner, S. Gupta, J.-R. Kim, and J.-P. Muller (2012), Hydraulic modeling of a distributary channel of Athabasca Valles, Mars, using a high-resolution digital terrain model, *J. Geophys. Res.*, *117*, E03009, doi:10.1029/2011JE003939.
- Meresse, S., F. Costard, N. Mangold, P. Masson, G. Neukum, and H. C.-I. Team (2008), Formation and evolution of the chaotic terrains by subsidence and magmatism: Hydrotes Chaos, Mars, *Icarus*, *194*(2), 487–500, doi:10.1016/j.icarus.2007.10.023.
- Milazzo, M. P., L. P. Keszthelyi, W. L. Jaeger, M. Rosiek, S. Mattson, C. Verba, R. A. Beyer, P. E. Geissler, A. S. McEwen, and R. T. Hi (2009), Discovery of columnar jointing on Mars, *Geology*, *37*(2), 171–174, doi:10.1130/g25187a.1.
- Miller, M., I. McCave, and P. Komar (1977), Threshold of sediment motion under unidirectional currents, *Sedimentology*, *24*(4), 507–527.
- O'Connor, J. E. (1993), Hydrology, hydraulics, and geomorphology of the Bonneville flood, *Geol. Soc. Am., Spec. Pap.*, *274*, 1–84.
- O'Connor, J. E., and V. R. Baker (1992), Magnitudes and implications of peak discharges from glacial Lake Missoula, *Geol. Soc. Am. Bull.*, *104*(3), 267–279.
- Pacifici, A., G. Komatsu, and M. Pondrelli (2009), Geological evolution of Ares Vallis on Mars: Formation by multiple events of catastrophic flooding, glacial and periglacial processes, *Icarus*, *202*(1), 60–77, doi:10.1016/j.icarus.2009.02.029.
- Pagliara, S., W. H. Hager, and H.-E. Minor (2006), Hydraulics of plane plunge pool scour, *J. Hydraul. Eng.*, *132*(5), 450–461, doi:10.1061/(ASCE)0733-9429(2006)132.
- Parker, G. (1978), Self-formed straight rivers with equilibrium banks and mobile bed. Part 2. The gravel river, *J. Fluid Mech.*, *89*(01), 127–146.
- Parker, G., P. R. Wilcock, C. Paola, W. E. Dietrich, and J. Pitlick (2007), Physical basis for quasi-universal relations describing bankfull hydraulic geometry of single-thread gravel bed rivers, *J. Geophys. Res.*, *112*, F04005, doi:10.1029/2006JF000549.
- Parker, T. J., R. S. Saunders, and D. M. Schneeberger (1989), Transitional morphology in west Deuteronilus Mensae, Mars: Implications for modification of the lowland/upland boundary, *Icarus*, *82*(1), 111–145.
- Pelletier, J. D., and V. R. Baker (2011), The role of weathering in the formation of bedrock valleys on Earth and Mars: A numerical modeling investigation, *J. Geophys. Res.*, *116*, E11007, doi:10.1029/2011JE003821.
- Petroff, A. P., O. Devauchelle, D. M. Abrams, A. E. Lobkovsky, A. Kudroli, and D. H. Rothman (2011), Geometry of valley growth, *J. Fluid Mech.*, *673*, 245–254, doi:10.1017/s002211201100053x.
- Pillans, B. (1985), Drainage initiation by subsurface flow in South Taranaki, New Zealand, *Geology*, *13*(4), 262–265.
- Rathburn, S. L. (1993), Pleistocene cataclysmic flooding along the Big Lost River, east central Idaho, *Geomorphology*, *8*(4), 305–319.
- Richardson, K., and P. A. Carling (2006), The hydraulics of a straight bedrock channel: Insights from solute dispersion studies, *Geomorphology*, *82*(1), 98–125, doi:10.1016/j.geomorph.2005.09.022.

- Roberts, S., O. Nielsen, D. Gray, and J. Sexton (2009), *ANUGA User Manual*, 117 pp., Geoscience Australia and Australian National Univ., Canberra.
- Robinson, M. S., and K. L. Tanaka (1990), Magnitude of a catastrophic flood event at Kasei Valles, Mars, *Geology*, *18*(9), 902–905, doi:10.1130/0091-7613(1990)018.
- Rotto, S., and K. L. Tanaka (1995), Geologic/geomorphologic map of the Chryse Planitia region of Mars, scale 1:5,000,000, U.S. Geol. Surv. Misc. Invest. Map, I-2441-A.
- Rouse, H. (1936), Discharge characteristics of the free overfall: Use of crest section as a control provides easy means of measuring discharge, *Civ. Eng.*, *6*(4), 257–260.
- Ruff, S. W., and P. R. Christensen (2002), Bright and dark regions on Mars: Particle size and mineralogical characteristics based on Thermal Emission Spectrometer data, *J. Geophys. Res.*, *107*(E12), 5127, doi:10.1029/2001JE001580.
- Schumm, S., K. Boyd, C. Wolff, and W. Spitz (1995), A ground-water sapping landscape in the Florida Panhandle, *Geomorphology*, *12*(4), 281–297.
- Scott, W. E. (1982), Surficial geologic map of the eastern Snake River Plain and adjacent areas, 111 to 115 west, Idaho and Wyoming, scale 1:250,000, U.S. Geol. Surv. Open File Rep., 81-507.
- Seidl, M. A., J. K. Weisell, and L. F. Pratson (1996), The kinematics and pattern of escarpment retreat across the rifted continental margin of SE Australia, *Basin Res.*, *8*(3), 301–316.
- Seminara, G., and M. Tubino (1989), Alternate bars and meandering, in *River Meandering*, edited by S. Ikeda and G. Parker, pp. 267–320, AGU, Washington, D. C.
- Shean, D., J. Fahle, M. Malin, L. Edwards, and L. Posiolova (2011), MRO CTX stereo image processing and preliminary DEM quality assessment, paper presented at Lunar Planet. Sci. Conf.
- Shields, A. (1936), *Anwendung der Aehnlichkeitsmechanik und der Turbulenzforschung auf die Geschiebebewegung*, 36 pp., Preussischen Versuchsanstalt fur Wasserbau, Berlin.
- Stein, O., and P. Julien (1993), Criterion delineating the mode of headcut migration, *J. Hydraul. Eng.*, *119*(1), 37–50.
- Stein, O., P. Julien, and C. Alonso (1993), Mechanics of jet scour downstream of a headcut, *J. Hydraul. Res.*, *31*(6), 723–738.
- Tinkler, K. (1997), Critical flow in rockbed streams with estimated values for Manning's n, *Geomorphology*, *20*(1), 147–164.
- Tomasson, H. (2002), Catastrophic floods in Iceland, in *Extremes of the Extremes: Extraordinary Floods*, edited by A. Snorrason, H. Finnsdottir, and M. Moss, pp. 121–126, Intl. Assoc. of Hydrolog. Sci., Reykjavik, Iceland.
- Trampush, S., S. Huzurbazar, and B. McElroy (2014), Empirical assessment of theory for bankfull characteristics of alluvial channels, *Water Resour. Res.*, *50*(12), 9211–9220, doi:10.1002/2014WR015597.
- Vigilar, G., and P. Diplas (1997), Stable channels with mobile bed: Formulation and numerical solution, *J. Hydraul. Eng.*, *123*(3), 189–199.
- Vigilar, G., and P. Diplas (1998), Stable channels with mobile bed: Model verification and graphical solution, *J. Hydraul. Eng.*, *124*(11), 1097–1108.
- Villanueva, G., M. Mumma, R. Novak, H. Kaufi, P. Hartogh, T. Encrenaz, A. Tokunaga, A. Khayat, and M. Smith (2015), Strong water isotopic anomalies in the Martian atmosphere: Probing current and ancient reservoirs, *Science*, *348*(6231), 218–221, doi:10.1126/science.aaa3630.
- Wang, C. Y., M. Manga, and J. C. Hanna (2006), Can freezing cause floods on Mars?, *Geophys. Res. Lett.*, *33*, L20202, doi:10.1029/2006GL027471.
- Warner, N., S. Gupta, J.-P. Muller, J.-R. Kim, and S.-Y. Lin (2009), A refined chronology of catastrophic outflow events in Ares Vallis, Mars, *Earth Planet. Sci. Lett.*, *288*(1), 58–69, doi:10.1016/j.epsl.2009.09.008.
- Warner, N. H., S. Gupta, J.-R. Kim, S.-Y. Lin, and J.-P. Muller (2010), Retreat of a giant cataract in a long-lived (3.7–2.6 Ga) Martian outflow channel, *Geology*, *38*(9), 791–794, doi:10.1130/G31268.1.
- Williams, R. M., and M. C. Malin (2004), Evidence for late stage fluvial activity in Kasei Valles, Mars, *J. Geophys. Res.*, *109*, E06001, doi:10.1029/2003JE002178.
- Williams, R. M., R. J. Phillips, and M. C. Malin (2000), Flow rates and duration within Kasei Valles, Mars: Implications for the formation of a Martian ocean, *Geophys. Res. Lett.*, *27*(7), 1073–1076, doi:10.1029/1999GL010957.
- Wilson, L., G. J. Ghatan, J. W. Head, and K. L. Mitchell (2004), Mars outflow channels: A reappraisal of the estimation of water flow velocities from water depths, regional slopes, and channel floor properties, *J. Geophys. Res.*, *109*, E09003, doi:10.1029/2004JE002281.
- Wohl, E. E. (1992), Bedrock benches and boulder bars: Floods in the Burdekin Gorge of Australia, *Geol. Soc. Am. Bull.*, *104*(6), 770–778.
- Yalin, M. S., and E. Karahan (1979), Inception of sediment transport, *J. Hydraul. Div.*, *105*(11), 1433–1443.
- Zegers, T. E., J. H. P. Oosthoek, A. P. Rossi, J. K. Blom, and S. Schumacher (2010), Melt and collapse of buried water ice: An alternative hypothesis for the formation of chaotic terrains on Mars, *Earth Planet. Sci. Lett.*, *297*(3–4), 496–504, doi:10.1016/j.epsl.2010.06.049.

Erratum

In the originally published version of this article, there was an error in Figure 3 and a typo in the related captions. The figure has been replaced and the typo has been changed from “dimensionless 1-D stress” to “normalized upstream stress.” These modifications do not change the conclusions of this article. This version may be considered the authoritative version of record.